Finite Element–Based Stability Charts for Underground Cavities in Soft Calcarenites

M. Perrotti[1]; P. Lollino[2]; N. L. Fazio[3]; L. Pisano[4]; G. Vessia[5]; M. Parise[6]; A. Fiore[7]; and M. Luisi[8]

[1]*Research Assistant, Istituto di Ricerca per la Protezione Idrogeologica–Consiglio Nazionale delle Ricerche, via Amendola 122/I, Bari 70126, Italy (corresponding author). E-mail: m.perrotti@ba.irpi.cnr.it*

[2]*Researcher, Istituto di Ricerca per la Protezione Idrogeologica– Consiglio Nazionale delle Ricerche, via Amendola 122/I, Bari 70126, Italy. E-mail: p.lollino@ba.irpi.cnr.it*

[3]*Research Assistant, Istituto di Ricerca per la Protezione Idrogeologica– Consiglio Nazionale delle Ricerche, via Amendola 122/I, Bari 70126, Italy. E-mail: n.fazio@ba.irpi.cnr.it*

[4]*Research Assistant, Istituto di Ricerca per la Protezione Idrogeologica–Consiglio Nazionale delle Ricerche, via Amendola 122/I, Bari 70126, Italy. E-mail: l.pisano@ba.irpi.cnr.it*

[5]*Researcher, Univ. di Chieti-Pescara "G. D'Annunzio," Via dei Vestini, 31, Chieti 66100, Italy. E-mail: giovanna.vessia@unich.it*

[6]*Associate Professor, Università degli Studi di Bari "Aldo Moro," Via Orabona, 4, Bari 70125, Italy; formerly, Research Associate, Istituto di Ricerca per la Protezione Idrogeologica–Consiglio Nazionale delle Ricerche, via Amendola 122/I, Bari 70126, Italy. E-mail: m.parise@ba.irpi.cnr.it*

[7]*Geologist, Autorità di Bacino Puglia, Bari, Strada Provinciale per Casamassima km 3, Valenzano 70010, Italy. E-mail: antonello.fiore@adb .puglia.it*

[8]*Engineer, Autorità di Bacino Puglia, Bari, Strada Provinciale per Casamassima km 3, Valenzano 70010, Italy. E-mail: michele.luisi@adb.puglia.it*

Abstract: The stability of shallow, artificial underground cavities in soft rocks interacting with overlying structures and infrastructures represents a challenging problem to be faced. This paper discusses a methodology that can be useful for a preliminary stability assessment of underground cavities in soft calcarenites based upon the results of parametric two-dimensional (2D) and three-dimensional (3D) finite-element analysis of ideal underground cavities. The study aimed at exploring those relationships between the geometrical parameters of the cave system and the strength properties of the rock material to define charts that can be useful to evaluate the stability of the rock mass. Moreover, the influence of three-dimensionality was also accounted for based on 3D parametric analyses with variable cavity length and the comparison with the results of the corresponding 2D analyses.

Introduction

The stability of artificial underground cavities in soft rocks represents a challenging problem to be faced, particularly when the cavities are located at a shallow depth with a high possibility of interacting with the above structures or infrastructures in urban areas (Aydan et al. 2005; Parise and Lollino 2011; Lollino et al. 2013). In the past, this problem has been frequently underestimated or even neglected during land management and planning activities, and the consequence is that structures and transport lines nowadays frequently sit directly above the existing cavities, or in the areas potentially affected by instability problems occurring therein. Moreover, soft porous rocks are

generally highly susceptible to degradation processes due to the effects of weathering induced by climatic factors (water infiltration, humidity, cavity submersion, etc.) under either a monotonic or cyclic process, as well as in the short and long term (Aydan et al. 2005; Andriani and Walsh 2010; Hall et al. 2010; Ciantia et al. 2015). As a consequence, soft rocks tend to reduce their strength with time due to the microcracking propagation through the rock mass, so that the risk to the overlying built-up environment induced by the presence of the cavities increases with time, accordingly. The problem of assessing the stability of underground cavities in soft rocks is generally faced by means of approaches characterized by different levels of accuracy and reliability. Early-warning systems aimed at predicting the potential collapse of underground cavities through microseismic noise monitoring are becoming popular in high-risk areas and represent one of the most promising methods to provide very sensitive volumetric monitoring over single cavities (Evangelista et al. 2003; Aydan et al. 2005; Contrucci et al. 2011). Nonetheless, such a technique cannot help to control the stability conditions of a large number of cavities located in a specific area, as in the case of the underground environments of urbanized areas. In addition, the monitoring activity needs complex operations for the elaboration and the interpretation of the microseismic signals, which is not straightforward. Hence, different approaches need to be applied to predict the stability of high-density networks of underground cavities through variables that are easy to measure. To address this task, phenomenological and analytical approaches are generally chosen in the preliminary stage of the analysis to deduce if the rock mass is close to instability or not (Gesualdo et al. 2001; Fraldi and Guarracino 2009; Carter 2014). Later on, more deterministic and accurate approaches should be adopted, such as those based on numerical modeling (Bekendam 1998; Goodings and Abdulla 2002; Ferrero et al. 2010; Parise and Lollino 2011; Lollino et al. 2013). The latter approach can be very useful nowadays, because three-dimensional (3D) studies can be carried out due to the availability of powerful numerical codes, which are capable of treating a wide range of problems related to the structural features of the rock mass examined (for both continuous or discontinuous rock mass). However, although remaining the most efficient way to face stability problems, sophisticated numerical techniques cannot be applied to all cases of stability assessments because they require a wide set of input data, which are not frequently available. On the opposite, wide regions throughout the world are characterized by a huge number of cavities affecting the underground environment, so that numerical analyses cannot be pursued efficiently due to the large number of cases to be studied. Therefore, in such cases, defining some general criteria to be summarized in user-friendly charts aimed at providing a preliminary indication on the stability of the underground system could be very useful. For instance, Evangelista et al. (2003) and Federico and Screpanti (2003) tried to define simplified charts forthe assessment of the stability of a large number of cavities as a function of their geometrical and mechanical parameters, respectively, for the underground environments of the towns of Naples and Rome (Italy) based on the results of finite-element studies. Suchowerska et al. (2012) performed a wide series of finite-element calculations to derive stability charts of cavities excavated in fractured rocks by using the Hoek and Brown (Hoek and Brown 1997) failure criterion. Of course, it is crucial to remark that these approaches should be considered as a preliminary stage of the stability assessment, provided that reliable values of the compression and tensile strength of the rock mass under study are available, so that in the case of assessments indicating a medium to high level of hazard, more detailed and site-specific investigations must necessarily be applied.

The present work aimed at proposing and discussing a methodology that could be useful for the preliminary stability assessment of underground cavities in soft calcarenites based upon the results of a large number of parametric two-dimensional (2D) finite-element analyses of ideal cases of underground cavities and, therefore, based on a deterministic approach. In particular, the results of a study

aimed at assessing the stability of artificial underground cavities in the Apulia region of Southern Italy as a function of specific geometrical parameters of the problem, as well as of mechanical parameters of the rock masses surrounding the cavities, are here presented. Throughout Apulia, a large number of cavities have been excavated in the last century for soft calcarenite exploitation purposes and abandoned afterward; in recent years, several collapses affected some of these cavity systems, involving structures and roads located at the ground surface and, therefore, inducing high risk for human life and properties. This study was aimed at exploring the relationships among the geometrical parameters of the cave system and the strength properties of the rock material cropping out in the examined area to define charts useful for preliminarily evaluating the stability of the rock mass. It took into account only cavities characterized by regular geometrical sections, as square or rectangular, within intact and continuous rock masses, whereas natural cavities with a complex 3D geometry and a clear anisotropic rock behavior due to the existence of persistent joints were not accounted for. In particular, the assumptions adopted, the methodologies used, and the results obtained by means of 2D and 3D finite-element analyses are discussed in the following sections, aiming at:

1. following the evolution of the stress-strain states of the rock masses affected by artificial underground cavities, up to the triggering of the failure process; and

2. searching eventual relationships existing among the geometrical factors and the rock mechanical parameters predisposing the failure of the rock mass.

The finite-element analyses were carried out by varying the values of the geometrical parameters within ranges typically observed for a large data set of underground cavities in Apulia, and those of the geotechnical properties within ranges typically measured for the calcarenites cropping out in the region. Therefore, the purpose of the analyses was to investigate the threshold value of the rock strength mobilized at the triggering stage of failure of the rock–cavity system, and the associated failure mechanism. The paper is structured as follows: the geological context of the examined region and the typical geomechanical properties of outcropping calcarenites are first presented; then, the assumptions adopted in the 2D finite-element analyses for single rectangular cavities, and the consequent results, are discussed to derive suitable stability charts. Later on, 3D sensitivity analyses of rectangular cross-section tunnels as a function of the cavity length are proposed to explore the role of the third dimension to ensure stability. The results from 2D (i.e., under plane-strain conditions) and 3D analyses are eventually compared.

Geological Context: Network of Artificial Underground Cavities in Apulia

In Apulia, sinkholes are the most peculiar typology of geological hazards (Parise and Lollino 2011; Parise and Vennari 2017), being related to the presence of underground voids of natural origin, due to the karst solutional processes that affect the soluble rocks widespread in the region, or caused by artificial activities, through excavation of anthropogenic cavities. In the last years, a threatening increase of sinkhole events has been registered, particularly related to anthropogenic cavities. Apulia has been well known for a long time for the occurrence of such events as experienced, for instance, during the crises that hit the towns of Canosa di Puglia and Andria during the 1970s and 1980s. Starting in the first years of the present century, the frequency of events had a clear increment, which reached a peak during 2009 and 2010. It should also be noted that the documented events in Apulia, so far at a total number of approximately 150 (Parise and Vennari 2013; Parise et al. 2013b), represent only a small part of what actually occurs, because many others (likely the majority) are not registered

due to lack of information, or due to rapid infilling of sinkholes by the landowners. Concerning the different categories of artificial cavities [according to the classification by Parise et al. (2013a)], which are responsible for the development of sinkholes at the surface, the most dangerous are by far represented by quarries and mines (Parise 2010, 2016). Extraction of calcarenite rocks, to be used as building materials, was often carried out in Apulia through the opening of underground quarries, thus allowing use of the ground surface for agricultural practices. This caused the widespread presence of cavities at variable depths, typically located at the peripheries of urban areas, which were abandoned later on once the production phase stopped (Parise 2012, 2015). With time, the urban expansion brought the towns just above those sites, thus highly increasing the risk of sinkhole development affecting the built-up areas (Lollino et al. 2013; Pepe et al. 2013).

Geomechanical Characterization of Calcarenites

The underground cavities examined here were excavated within deposits of soft calcarenites, widespread throughout Apulia. The rocks can be classified from very soft to extremely soft based on the values of the uniaxial compressive strength (Bieniawski and Bernede 1979; Dobereiner and De Freitas 1986), as described later in detail. The typical low values of this mechanical feature represent the main cause for the wide use in the construction field as a building material due to the ease in extraction and workability of this material. In general, the calcarenite deposits cropping out in Apulia can be ranked into four main geological groups as shown in Fig. 1:

• Miocene calcarenites,

• Pliocene calcarenites,

• Gravina calcarenites (Pleistocene), and

• terraced marine deposits (Quaternary).

Because the majority of the Apulian underground cavities have been excavated within the Gravina calcarenites and the Miocene calcarenites, the mechanical properties of these formations are taken into account in the present study. The Gravina calcarenites are characterized by low and variable values of the uniaxial compressive strength under dry conditions, ranging between 1 and 9 MPa (Coviello et al. 2005; Andriani and Walsh 2010; Ciantia et al. 2015). The degree of saturation significantly affects the rock strength, so that under full saturation conditions (Sr = 100%), the uniaxial compressive strength decreases, with rates higher than 50% with respect to the dry material, in the range 0.36 MPa (Andriani and Walsh 2010; Ciantia et al. 2015). The tension strength, measured by means of indirect tension tests, generally ranges between 0.2 and 2.0 MPa (Coviello et al. 2005; Andriani and Walsh 2010; Ciantia et al. 2015). Therefore, the ratio between uniaxial compressive and tension strength is approximately equal to 3–12. The Miocene calcarenites, in contrast, exhibit uniaxial compressive strength values generally higher than those of the Gravina calcarenites. In dry conditions, these values cover the interval between 10 and 22 MPa (Andriani and Walsh 2010), and after saturation, they tend to decrease as well. The aforementioned ranges need to be considered as approximate, because petrographical and structural differences in the geological formations influence the mechanical responses of the rock masses and assign quite a high degree of heterogeneity in their behavior among different study sites. Furthermore, the weathering processes related to both the chemical-physical agents and the drying-wetting cycles induce mechanical degradation, and therefore, the rock strength values tend to decrease accordingly. As in the case of the saturation processes, weathering can, therefore, bring the calcarenite mass around the cavity to the failure conditions in the long term.

2D Parametric Finite-Element Analyses

Threshold Stability for a Single Cavity of Rectangular Shape

A large set of 2D finite-element analyses were carried out for ideal schemes of rectangular cavities with variable geometrical parameters considered as representative of the typical geometries of the artificial underground cavities throughout the Apulia region. The analyses were performed using the PLAXIS 2D software. The analysis domain consisted of a 100-m-wide and 60-m-high rectangle as shown in Fig. 2(a), these sizes being much larger than those of the cavity to reduce the risk of boundary effects. Fig. 2(a) also reports the adopted discretization mesh, which is a compromise between the need for calculation accuracy in the area of interest (i.e., around the cavity) and the need for reducing the computational costs. To reach a sufficient calculation accuracy in the mesh area where higher strain gradients would have been expected, a highly refined mesh (average element size approximately 0.1 m2) was chosen in the area around the cavity, whereas coarser elements were chosen in the areas far from the cavity. From a geometrical point of view, the rectangular cavity is defined in Fig. 2(b) by means of three Fig. 1. Calcarenite deposits cropping out in Apulia (adapted from Lepore et al. 2014) features: the cavity width (L), the cavity height (h), and the overburden thickness, also called depth. The boundary conditions prescribed to the domain were as follows:

• Zero horizontal displacement along the lateral sides,

• Zero vertical and horizontal displacement along the bottom of the mesh, and

• Free displacement along the ground surface.

All analyses were performed under drained conditions, with no pore-water pressure allowed to develop in the material. The numerical analyses were performed according to three calculation stages:

• First stage: initialization of the stress state within the rock mass domain. This was pursued by assigning a K0 value equal to 1, with the vertical stress being calculated by means of the gravitational forces. Assume a K0 value equal to 1 is considered here as conservative, because higher values have been generally observed to increase the stability of the cavity roofs. Lower values of K0 are unlikely to be measured for shallow rock masses (Brown and Hoek 1978; Gonzalez De Vallejo and Hijazo 2008).

• Second stage: elastic-plastic computation based on the chosen constitutive model (described hereafter) and the assignment of the mechanical properties to the calcarenite.

• Third stage: simulation of the cavity excavation. At this stage, the portion of the domain within the cavity was deactivated, and a new plastic calculation was performed. It is worthwhile to note that, since no clear information on the in situ actual excavation sequence was available, a single excavation stage was adopted, representing a conservative assumption.

The purpose of the analyses was to evaluate, for the specific cavity geometry examined, the set of strength values of the rock material that gives rise to a failure mechanism, either local or general. To this aim, the general failure mechanism was represented by the development of a proper sinkhole (Waltham et al. 2005; Gutierrez et al. 2014) (i.e., a failure mechanism that starts from the cavity boundary and propagates upward, thus involving the rock mass portions immediately below the ground surface). Local failure mechanisms were instead characterized by the propagation of arch-shaped plastic zones on the cavity roof or, as an alternative, by plastic zones along the lateral walls of the cavity. From a numerical standpoint, the generation of a whole failure mechanism, either local or general, was detected by means of the combination of the following criteria:

• Lack of numerical convergence,

• Generation of a closed yielding mechanism involving a well-defined rock volume delimited by clear plastic zones or deviatoric strains, and

• Vertical displacements of selected nodes belonging to the mesh region involved in the failure mechanism increasing with numerical time steps.

An elastic perfectly plastic constitutive model characterized by a Hoek-Brown failure criterion, as shown in Fig. 3 [modified from Hoek and Martin (2014)], was chosen to simulate the rock mechanical behavior. This choice complies with the need for simulating a nonlinear strength envelope in Mohr's plane, as generally observed for calcarenite rocks. Furthermore, the parameters of this model can be more easily derived from the basic laboratory tests commonly used in rock mechanics, such as the uniaxial compressive and indirect tensile tests (Hoek and Brown 1997). The Hoek-Brown model requires the parameters reported in Table 1. It is worthwhile pointing out that, to avoid overestimation of the rock shear strength, a non-associated flow rule (dilatancy angle c = 0) was adopted (Vermeer and De Borst 1984). The main variable chosen in the parametric analyses was the threshold value of uniaxial compressive strength ($\sigma_{c,min}$), which corresponded to the activation of a failure mechanism for each single cavity geometry. The rock mass was assumed to be intact and not affected by discontinuities, so that a geological strength index GSI (Hoek 1994) value equal to 100 was used in the analyses. This assumption complied with the several field surveys performed in situ, which confirmed how these rock masses are only rarely jointed. It follows that the results obtained from the analyses cannot be considered valid for those cases where the rock mass is characterized by single joints or joint sets, which might assign a certain degree of anisotropy to the rock mass and influence the mass stability. The parameter D, representative of the disturbance factor induced by the excavation technique, was equal to zero to simulate a rock mass that has not been disturbed or affected by stress release processes due to the specific excavation technique, which was represented by hand-excavation techniques throughout the study region. The parameter mi was defined in accordance with the suggestions proposed by Cai (2010), and as a first approximation, it can be considered as representative of the ratio between the uniaxial compressive and tensile strength of the rock. Fig. 4 indicates that an increase of mi gives rise to a reduction of the tensile strength and an increase of the average slope of the strength envelope, as already noted by Hoek (1983). Here, the mi value was chosen in accordance with the values proposed by Hoek (2007) for the specific rock typology, as well as with the results of uniaxial compressive and tensile strength tests performed on samples belonging to different varieties of the Gravina calcarenite formation (Andriani and Walsh 2010). Therefore, numerical analyses assuming values of mi equal to 3, 8, and 16 were performed, and the comparison among the corresponding results is discussed here.

Because the GSI, D, and mi values were prescribed as constant in the analyses, the uniaxial compressive strength (σ_c) was considered as a variable dependent on three geometrical parameters, which were L, t, and h [Fig. 2(b)], to derive the threshold value ($\sigma_{c,min}$) that corresponded to the triggering of a local or global failure mechanism. Thus, the relationships among the threshold value of uniaxial compressive rock strength ($\sigma_{c,min}$) and the geometrical features of the cavity were investigated. For the sake of simplicity, no surcharge was assumed along the ground surface, so that the value of the vertical stress at the depth of the cavity roof before excavation was assumed to be equal to the value of the rock unit weight (g) multiplied by the depth (t). The numerical results were reported in plots showing the $\sigma_{c,min}/\ \sigma_v$ ratio, which was the ratio between the threshold value of uniaxial compressive strength mobilized at failure and the vertical stress before excavation at the depth of the cavity roof, as a function of the nondimensional ratio L/t, here called the width-to-depth

ratio. The $\sigma_{c,min}/\sigma_v$ – L/t curves were drawn by keeping the ratio L/h, which was the shape ratio of the cavity, as constant. An example of this plot type is shown in Fig. 5.

A typical example of the locus representative of the combinations of the geometrical features and the rock threshold strength is Fig. 4. Influence of the mi parameter on Hoek-Brown strength envelope (adapted from Cai 2010) Table 1. Values of Hoek-Brown Parameters Assigned in 2D Analyses Parameter Adopted value represented by the dotted curve in Fig. 5; a point lying above the curve means that the cavity is supposed to be stable, or conversely, a point below this line represents a possible instability. Such a stability chart could eventually be used to calculate the A segment, that is, the safety margin with respect to failure. It is the ratio between the actual in situ value of the rock uniaxial compressive strength (σ_c) and the threshold value for stability of the same parameter ($\sigma_{c,min}$) at the same value of the ratio L/t. Alternatively, the same plot enables calculation of the B segment, which is the maximum value of the width-to-depth ratio (L/t) allowed for stability, given the assigned value of the ratio between the in situ uniaxial compressive strength (σ_c) and the vertical stress (σ_v). The results of the analyses, assuming mi = 3, are reported in Fig. 6 in terms of curves representing $\sigma_{c,min}/\sigma_v$ as a function of L/t for different values of the shape ratio (L/h). The geometrical parameters considered in the analyses, which corresponded to the range of the typical geometrical features observed for the Apulian cavities, are as follows:

• L = variable between 1 and 30 m;

• h = 3, 5, and 7 m; and

• t = 2, 5, and 10 m.

All the curves represented in Fig. 6 showed an increase of the ratio $\sigma_{c,min}/\sigma_v$ with the increment of the ratio L/t, which means that higher-threshold strengths were needed for stability when the width-to-depth ratio increased. Moreover, all curves seemed to be very similar, regardless of the values of the shape ratio (L/h). This suggests that, with the assumed value of mi (mi = 3), the shape ratio provided a negligible influence on the threshold envelope.

The curves obtained for mi = 8 are instead reported in Fig. 7. The trend of the curves was similar to those in Fig. 6, but in this case, larger values of $\sigma_{c,min}/\sigma_v$ with respect to the previous case were observed at large values of L/t. The plot in Fig. 7 highlights that, for values of the ratio L/t lower than 1.5, the shape factor provided a limited influence, whereas for higher values, the ratio $\sigma_{c,min}/\sigma_v$ tended to increase also with the L/h ratio for the same values of L/t. The results of the analyses obtained by assuming mi = 16 are depicted in Fig. 8. Again, the trend of the curves followed the same increment of the ratio $\sigma_{c,min}/\sigma_v$ with the ratio L/t, but $\sigma_{c,min}/\sigma_v$ values significantly larger than those in Figs. 6 and 7 were observed at large values of the ratio L/t. A remarkable influence of the shape factor (L/h) was observed in this case, so that the influence of L/h appeared already for values of the ratio L/t higher than 1 and increased with the higher values of L/t. The effect of the mi parameter was clarified if the same results were plotted by grouping together the curves with the same L/h values and different mi. Figs. 9(a–d) clearly show that, at the same value of L/t, the $\sigma_{c,min}/\sigma_v$ values increased with mi. However, this effect was still limited at L/h values lower than 1 and became more evident with higher L/h values. This result might be related to the high value of the tensile strength corresponding to a low value of mi, such as in the case of mi = 3, so that at L/t values larger than 1.5, a larger tensile strength value increased the overall stability of the cavity roof against instability processes that can typically develop for thin-beam roof schemes (long-span and low roof thickness) undergoing flexural behavior, as described in detail in the next section. This result highlighted the importance of an

accurate estimation of the mi parameter value from Hoek-Brown criterion when assessing the stability of an underground cavity.

Influence of Geometrical Features on the Failure Mechanism

Numerical analyses were also carried out to assess the influence of the geometrical features of the cavity on the failure mechanism. The investigated geometrical features were the shape factor (L/h) and the width-to-depth ratio (L/t) as previously defined. In particular, according to the numerical results, three different failure mechanisms were identified:

1. *Arch-shaped general failure*: This mechanism is formed by plastic shear zones that, as a whole, resemble a portion of an arch that does not reach the ground surface. This failure mechanism needs a sufficiently thick roof above the cavity that allows for the generation of a compression arch that resists against the acting stress field; arch-shaped general failure mechanism is shown in Fig. 10(a).

2. *Beam-shaped general failure*: For this mechanism, plastic shear zones start from the upper lateral edges of the cavity and propagate upward toward the ground surface, where the formation of a sinkhole collapse is generated (Waltham et al. 2005; Gutierrez et al. 2014); the beam-shaped general failure mechanism is reported in Fig. 10(b).

3. *Arch-shaped local failure*: This mechanism corresponds to a plastic shear mechanism involving a small portion in the middle of the cavity roof, as shown in Fig. 11. It does not imply a complete collapse of the cavity roof, but it generates fissures along the cavity roof. As a consequence, this mechanism is representative of a possible evolution toward two possible failure mechanisms, described at Point 1 or 2.

According to the numerical results, these failure mechanisms can be associated with well-defined combinations of the $\sigma_{c,min}/\sigma_v$ stability threshold values and cavity geometrical features, which in turn vary according to the adopted mi value. These results are shown in Figs. 12–14 according to the type of failure mechanism. In particular, in Fig. 12 (mi = 3), a transition from arch-shaped general failure to beam-shaped general failure was observed at L/t = 1.5. As a matter of fact, for L/t values lower than 1.5, which were representative of a thick beam roof, the failure mechanism was generally arch-shaped, whereas for higher values of L/t (thin-beam roof), the failure moved toward a typical mechanism of general shear failure. Moreover, for L/t ≥ 2, local arch-shaped failures developed, generally for $\sigma_{c,min}/\sigma_v$ values higher than those causing the general mechanism. The values of threshold strength, lying either to the right or to the left of L/t = 1.5 in Figure 12, depended on the values of the shape factor (L/h as shown by the interpolation lines. The ranges of the shape factor values corresponded to three different cases:

• L/h<1 (rectangular cavity, mostly developed in height, with L < h);

• L/h = 1 (square cavity, L = h); and

• L/h>1 (rectangular cavity, mostly developed laterally, with L > h).

Indeed, for L/t<1.5 (which was the failure domain of the general arch mechanism), the values of the ratio $\sigma_{c,min}/\sigma_v$ were higher for L/h<1 than those for L/h>1. This should be presumably related to the higher shape stiffness of a cavity characterized by a ratio height/width larger than 1. This was also confirmed for L/t>1.5, even though the effect related to the cavity shape tended to be lower or even negligible. The results obtained for the case mi = 3 were almost confirmed for mi = 8 in Fig. 13 and mi = 16 in Fig. 14, although some differences can be drawn from the comparison of the plots. In fact, the mechanism of arch-shaped local failure was clearly distinguished by the beam-shaped general

failure in terms of the $\sigma_{c,min}/\sigma_v$ ratio values corresponding to the same L/t values. However, the L/t threshold value dividing the arch-shaped and the beam-shaped failure still remained equal to L/t = 1.5 for the cases mi = 8 and mi = 16.

3D FEM Analyses

3D finite-element analyses were carried out for ideal schemes of rectangular cavities characterized by geometrical features identical to those of the 2D parametric analyses described earlier. The aim of the 3D analyses was to investigate the role of the third dimension in the general stability of the cavities as compared with the results of 2D analyses. The 3D numerical simulations were performed using PLAXIS 3D software. The 3D underground cavity was modeled with a parallelepiped volume characterized by width LT = 60 m, height H = 40 m, and length D = 60 m, as shown in Fig. 15(a). This size was significantly larger than the mean size of the cavity to reduce the risk of boundary effects that might affect the numerical results. The upper surface was representative of the horizontal ground surface. The cavity was simulated as composed by a variable number of volumes to be excavated, of constant length, and with a square or rectangular cross section; the geometrical features within the x,yplane (the same as those adopted for the 2D analyses) were designed in Fig. 15(b) as cavity width (L), height (h), and overburden thickness (t).

The influence of the cavity length (z-direction) on the cavity stability was investigated by simulating a progressive reduction of the cavity length starting from a maximum value of d = 60 m to a minimum of d = 5 m. The analyses were performed by taking into account three types of cavity cross sections with the following features:

• Square cross section: L = 5 m, h = 5 m, t = 5m;

• Rectangular cross section: L = 7.5 m, h = 5 m, t = 5 m; and

• Rectangular cross section: L = 10 m, h = 5m, t = 5 m.

The discretization mesh adopted for the numerical analyses is shown in Fig. 16 and is a compromise between the need for calculation accuracy in the area around the cavity and the need to reduce the computational costs. The 3D numerical analyses were performed with the same boundary conditions and according to the same three stages adopted in the 2D analyses (see the “Threshold Stability for a Single Cavity of Rectangular Shape” section). As for the 2D analyses, the aim of the analyses was to evaluate the threshold value of uniaxial compressive strength ($\sigma_{c,min}$) corresponding to a failure mechanism (e.g., sinkhole or local failure in the form of arc-shaped feature on the roof of cavity) for a specific cavity scheme. The same criteria for detecting the occurrence of failure adopted in the 2D analyses were also adopted for the 3D analyses. An elastic perfectly plastic constitutive model with a Hoek- Brown failure criterion was chosen to simulate the rock mechanical behavior. The values of the mechanical strength parameters are reported in Table 2. The results of 3D FEM analyses were then compared with the corresponding 2D analyses that assumed the same geometrical features in the x,y-plane. The simulation of the reduction of the cavity length (d) was pursued by reducing the model rock volume involved in the deactivation process, as shown in Fig. 17.The results obtained from the analyses referring to the cavity with a squared cross section (L = h = 5 m) are reported in Fig. 18 in terms of stability threshold value ($\sigma_{c,min}$) against cavity length (d). The interpolation curve indicated an increasing value of the threshold strength with the cavity length up to an asymptotic value approximately equal to that resulting from the 2D FEM analysis (σ_c = 130 kPa). In particular, when d = 5 m, failure of cavity was reached with $\sigma_{c,min}$ = 70 kPa, whereas with d = 60 m, failure occurred at $\sigma_{c,min}$ = 120 kPa, which was very close to the result obtained from the 2D analysis (130 kPa). This

result suggests that a 2D analysis can be representative of the actual geometry of the cavity only when the cavity is significantly long, with d approximately equal to 50–60 m, whereas it is conservative for lower cavity lengths. Results were in good agreement with the comparison between 3D caverns versus 2D tunnels (Pariseau 2011; Fazio et al. 2017). The failure mechanism associated with the cavity geometry L = h = t = 5 m was plotted in Figs. 19(a–d) in terms of plastic points, vertical displacements, and deviatoric strain contours. Fig. 19 shows that rock yielding involved the entire rock material around the cavity and propagated up to the ground surface with the generation of a typical sinkhole mechanism, whose center was approximately located in the middle sector of the cavity. For a cavity with a rectangular cross section (L = 7.5 m and h = t = 5 m), the threshold strength values to meet stable conditions are shown in Fig. 20 with respect to the cavity length. As for the previous case, the interpolating curve indicated a clear increment of the threshold strength with the cavity length up to an asymptotic value ($\sigma_{c,min}$ = 180 kPa), which was slightly lower than the value obtained from the corresponding 2D analysis ($\sigma_{c,min}$ = 205 kPa); with a value of d = 5 m, the failure of cavity was approximately reached with $\sigma_{c,min}$ = 80 kPa. Finally, the results in Fig. 21 refer to the case of a cavity with a rectangular cross section, L = 10 m wide and h = 5 m high (t = 5 m). The same trend observed in Figs. 18 and 20 was also obtained for this case, with an increasing value of the threshold uniaxial compressive strength ($\sigma_{c,min}$) with respect to the cavity length, up to an asymptotic value ($\sigma_{c,min}$ = 300 kPa) slightly lower than the corresponding one resulting from the 2D FEM analysis (that is, $\sigma_{c,min}$ = 320 kPa). The failure mechanism associated with the case with a cavity length equal to 20 m is reported in Figs. 22(a–d) in terms of plastic points, vertical displacements, and deviatoric strain contours. The failure mechanism indicated that rock yielding started from the roof of the cavity and propagated upward to reach the ground surface, forming a closed sinkhole in the middle of the cavity length.

Concluding Remarks

A large number of both 2D and 3D finite-element analyses were accomplished and presented in this study and then summarized into stability charts, which could be used for preliminary assessment of the stability of artificial underground cavities excavated within soft rock masses that can be modeled as homogeneous and intact. Concerning the 2D numerical results, the following three conclusions for the stability of the cavities can be drawn:

1. The threshold strength for stability of the cavity increased with the ratio L/t. For L/t<1.5, the arch-shaped general failure occurred, whereas for L/t>1.5, the beam-shaped general failure usually occurred. It follows that better stability conditions corresponded to the cases for which the cavity width was comparable with the depth.

2. The results previously described were independent of the mi values in terms of trend, although the absolute values of the ratio $\sigma_{c,min}/\sigma_v$ increased as mi increased from 3 to 16. 3. For low values of mi, the values of the shape ratio (L/h) did not affect either the failure mechanism or the values of $\sigma_{c,min}/\sigma_v$, whereas for large values of mi, $\sigma_{c,min}/\sigma_v$ increased with the shape ratio at large values of L/t. Thus, from the results of the 2D FEM simulations, only the L/t ratio affected the failure mechanism, whereas the mi parameter affected the strength ratio $\sigma_{c,min}/\sigma_v$: this latter increased as mi increased.

The comparison between the 2D and 3D numerical results showed that the third dimension was an additional source of strength, as the length of the cavity was short enough. In fact, as the cavity length increased, the threshold strength for stability tended to the corresponding value of the 2D model, which was different according to the shape of the cavity cross section. It should be pointed out that the results of this parametric study were affected by the simplifications adopted in the numerical

models examined and the approximations used to detect the failure occurrence within the numerical study. Therefore, the charts proposed in the study need to be validated by means of comparison with real case studies before being applied in the engineering practice, and this should be discussed in a future work to be proposed by the authors.

References

Andriani, G. F., and Walsh, N. (2010). "Petrophysical and mechanical properties of soft and porous building rocks used in apulian monuments (South Italy)." Geol. Soc., London, Spec. Publ., 333, 129–141.

Aydan, O., Tano, H., Sakamoto, A., Yamada, N., and Sugiura, K. (2005). "A real-time monitoring system for the assessment of stability and performance of in abandoned room and pillar lignite mines." Post-min. 2005, 38(11), 1–12.

Bekendam, R. F. (1998). "Pillar stability and large-scale collapse of abandoned room and pillar limestone mines in south-Limburg, the Netherlands." Ph.D. thesis, Univ. of Utrecht, Utrecht, Netherlands.

Bieniawski, Z. T., and Bernede, M. J. (1979). "Suggested methods for determining the uniaxial compressive strength and deformability of rock materials: Part 1. Suggested method for determining deformability of rock materials in uniaxial compression." Int. J. Rock Mech. Min. Sci. Geomech. Abstr., 16(2), 135–140.

Brown, E. T., and Hoek, E. (1978). "Trends in relationships between measured in-situ stresses and depth." Int. J. Rock Mech. Min. Sci. Geomech. Abstr., 15(4), 211–215.

Cai, M. (2010). "Practical estimates of tensile strength and Hoek–Brown strength parameter m i of brittle rocks." Rock Mech. Rock Eng., 43(2), 167–184.

Carter, T. G. (2014). "Guidelines for use of the scaled span method for surface crown pillar stability assessment" Ontario Ministry of Northern Development and Mines, 2010, pp. 1–34.

Ciantia, M. O., Castellanza, R., and Di Prisco, C. (2015). "Experimental study on the water-induced weakening of calcarenites." Rock Mech. Rock Eng., 48(2), 441–461.

Contrucci, I., Klein, E., Cao, N.-T., Daupley, X., and Bigarre, P. (2011). "Multi-parameter monitoring of a solution mining cavity collapse: First insight of precursors." C. R. Geosci., 343(1), 1–10.

Coviello, A., Lagioia, R., and Nova, R. (2005). "On the measurement of the tensile strength of soft rocks." Rock Mech. Rock Eng., 38(4), 251–273.

Dobereiner, L., and De Freitas, M. H. (1986). "Geotechnical properties of weak sandstones." Geotechnique, 36(1), 79–94.

Evangelista, A., Pellegrino, A., and Viggiani, C. (2003). "Cavità e gallerie nel Tufo Giallo Napoletano." Atti IX Ciclo Conf. MIR, Le opere in sotterraneo e il rapporto con l'ambiente, Patron Editore.

FALLA CASTELFRANCHI M. (1991) Pittura monumentale bizantina in Puglia.Milan, Italy.

Fazio, N., et al. (2017). "A three-dimensional back-analysis of the collapse of an underground cavity in soft rocks." Eng. Geol., 228, 301–311.

Federico, F., and Screpanti, S. (2003). “Effects of filling shallow room and pillar mines in weak pyroclastic rock.” Proc., XIII European Conference on Soil Mechanics and Geotechnical Engineering, Geotechnical Problems with Man-made and Man Influenced. Grounds, Prague, The Czech Republic.

Ferrero, A. M., Segalini, A., and Giani, G. P. (2010). “Stability analysis of historic underground quarries.” Comput. Geotech., 37(4), 476–486.

Fraldi, M., and Guarracino, F. (2009). “Limit analysis of collapse mechanisms in cavities and tunnels according to the Hoek–Brown failure criterion.” Int. J. Rock Mech. Min. Sci., 46(4), 665–673.

Gesualdo, A., Minutolo, V., and Nunziante, L. (2001). “Failure in Mohr–Coulomb soil cavities.” Can. Geotech. J., 38(6), 1314–1320.

Gonzalez de Vallejo, L. I., and Hijazo, T. (2008). “A new method of estimating the ratio between in situ rock stresses and tectonics based on empirical and probabilistic analyses.” Eng. Geol., 101(3–4), 185–194.

Goodings, D. J., and Abdulla, W. A. (2002). “Stability charts for predicting sinkholes in weakly cemented sand over karst limestone.” Eng. Geol., 65(2–3), 179–184.

Gutierrez, F., Parise, M., De Waele, J., and Jourde, H. (2014). “A review on natural and human induced geohazards and impacts in karst.” Earth Sci. Rev., 138, 61–88.

Hall, S., De Sanctis, F., Viggiani, G., and Evangelista, A. (2010). “Impiego della tecnica delle emissioni acustiche nella previsione dei dissesti in cavità: studi preliminari in laboratorio.” 2° convegno Sinkholes, ISPRA.

Primo Seminario “Stato dell’arte sullo studio dei fenomeni di sinkhloes e ruolo delle amministrazioni statali e locali nel governo del territorio,” Rome, Italy.

Hoek, E. (1983). “Strength of jointed rockmass.” Geotechnique, 33, 187–223.

Hoek, E. (1994). “Strength of rock and rock masses.” News J. ISRM, 2(2), 4–16.

Hoek E. (2007). “Practical rock engineering.” hhttps://www.rocscience .com/documents/hoek/corner/Practical-Rock-Engineering-Full-Text.pdf.

Hoek, E., and Brown, E. T. (1997). “Practical estimates of rock mass strength.” Int. J. Rock Mech. Min. Sci., 34(8), 1165–1186.

Hoek, E., and Martin, C. D. (2014). “Fracture initiation and propagation in intact rock–A review.” J. Rock Mech. Geotech. Eng., 6(4), 287–300.

Lepore, D., Spalluto, L., Fiore, A., Luisi, M., and Miccoli, M. N., (2014). “Distribuzione delle cavità antropiche nel territorio pugliese in relazione alle caratteristiche litostratigrafiche delle calcareniti neogeniche.” 3° Workshop Internazionale “Voragini in Italia,” ISPRA, Rome.

Lollino, P., Martimucci, V., and Parise, M. (2013). “Geological survey and numerical modeling of the potential failure mechanisms of underground caves.” Geosyst. Eng., 16(1), 100–112.

Parise, M. (2010). “The impacts of quarrying in the Apulian karst.” Advances in research in karst media, F. Carrasco, J.W. LaMoreaux, J. Duran, J. J. Valsero, and B. Andreo, eds., Springer, Berlin,441–447.

Parise, M. (2012). “A present risk from past activities: Sinkhole occurrence above underground quarries.” Carbonates Evaporites, 27(2), 109–118.

Parise, M. (2015). “A procedure for evaluating the susceptibility to natural and anthropogenic sinkholes.” Georisk, 9(4), 272–285.

Parise, M. (2016). “Modern resource use and its impact in karst areas–Mining and quarrying.” Zeitschrift Geomorphol., 60(2), 199–216.

Parise, M., Galeazzi, C., Bixio, R., and Dixon, M. (2013a). “Classification of artificial cavities: A first contribution by the UIS Commission.” Proc., 16th Int. Congress of Speleology, M. Filippi, and P. Bosak, eds., Czech Speleological Society, Praha, Czech Republic, Brno, 2, 230–235.

Parise, M., and Lollino, P. (2011). “A preliminary analysis of failure mechanisms in karst and man-made underground caves in Southern Italy.” Geomorphol., 134(1–2), 132–143.

Parise, M., and Vennari, C. (2013). “A chronological catalogue of sinkholes in Italy: The first step toward a real evaluation of the sinkhole hazard.” Proc., 13th Multidisciplinary Conf. on Sinkholes and the Engineering and Environmental Impacts of Karst, L. Land, D. H. Doctor, and B. Stephenson, eds., National Cave and Karst Research Institute, Carlsbad, NM, 383–392.

Parise, M., and Vennari, C. (2017). “Distribution and features of natural and anthropogenic sinkholes in Apulia.” Eurokarst 2016, Neuchatel. Advances in the hydrogeology of karst and carbonate reservoirs, P. Renard, and C. Bertrand, eds., Springer, Cham, Switzerland, 27–34.

Parise, M., Vennari, C., Guzzetti, F., Marchesini, I., and Salvati, P. (2013b). “Preliminary outcomes from a catalogue of natural and anthropogenic sinkholes in Italy, and analysis of the related damage.” Rendiconti online della società geologica italiana, 24, 225–227.

Pariseau, W. G. (2011). “Three-dimensional excavations.” Design analysis in rock mechanics, Chapter 7, CRC Press, Boca Raton, FL.

Pepe, P., Pentimone, N., Garziano, G., Martimucci, V., and Parise, M. (2013). “Lessons learned from occurrence of sinkholes related to man-made cavities in a town of southern Italy.” Proc., 13th Multidisciplinary Conf. on Sinkholes and the Engineering and Environmental Impacts of Karst, L. Land, D. H. Doctor, and B. Stephenson, eds., National Cave and Karst Research Institute, Carlsbad, NM, 393–401.

PLAXIS 2D [Computer software]. Plaxis, Delft, Netherlands.

PLAXIS 3D [Computer software]. Plaxis, Delft, Netherlands.

Suchowerska, A. M., Merifield, R. S., Carter, J. P., and Clausen, J. (2012). “Prediction of underground cavity roof collapse using the Hoek–Brown failure criterion.” Comput. Geotech., 44, 93–103.

Vermeer, P. A., and De Borst, R. (1984). “Non-associated plasticity for soils, concrete and rock.” Heron, 29(3), 1–64.

Waltham, T., Bell, F., and Culshaw, M. (2005). Sinkholes and subsidence, Springer, Chichester, U.K.

Tab. 1. Values of Hoek-Brown Parameters Assigned in 2D Analyses

Parameter	Adopted value
γ (kN/m3)	16
E' (MPa)	100
ν	0.3
σ_c (kPa)	Variable
GSI	100
Ψ (°)	0
m_i	3 – 8 – 16
D	0

Note: GSI = geological strength index

Table 2. Values of Hoek-Brown Model Parameter Assigned in 3D analyses

Parameter	Adopted value
γ (kN/m3)	16
E' (MPa)	100
ν	0.3
σ_c (kPa)	Variable
GSI	100
Ψ (°)	0
m_i	8
D	0

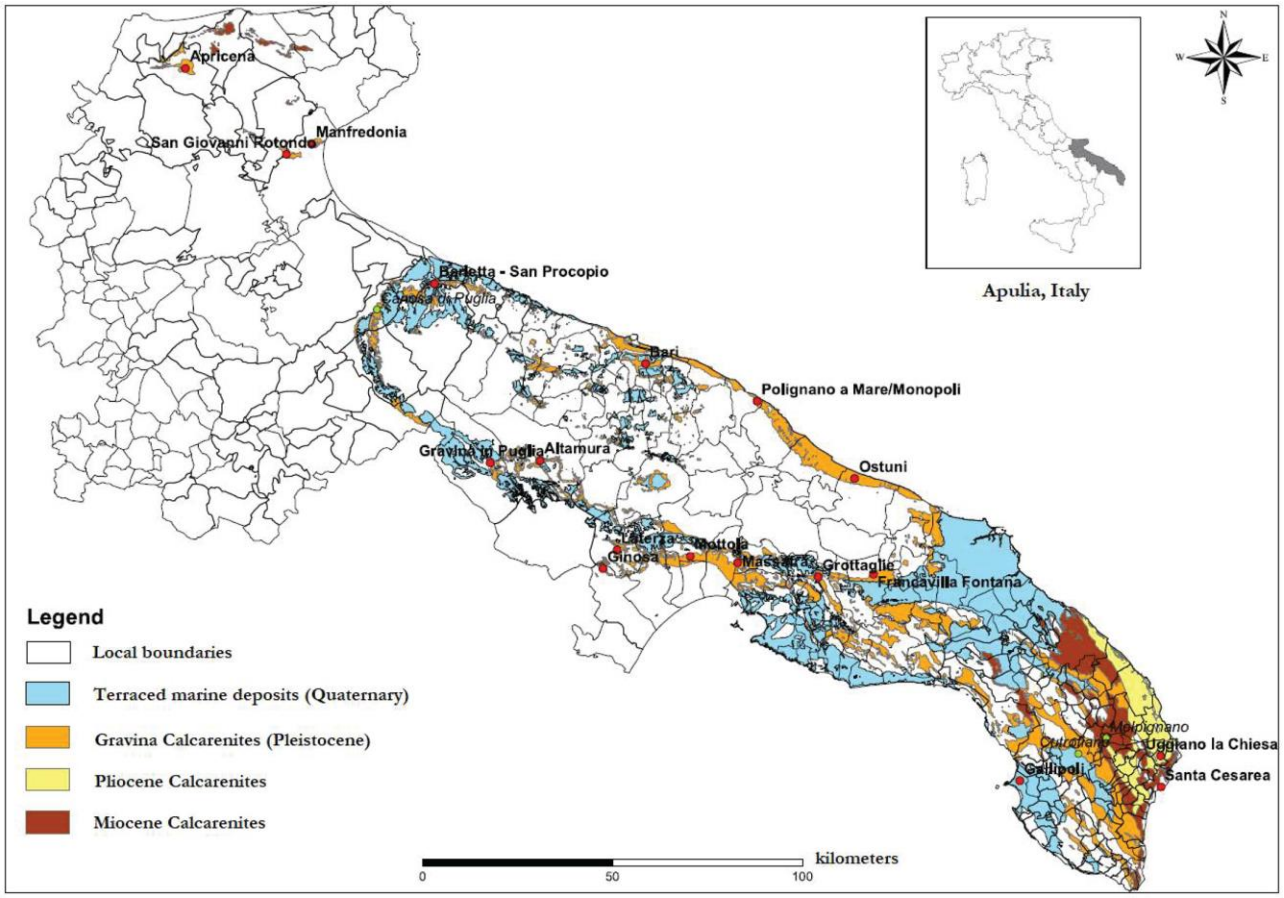

Fig. 1. Calcarenite deposits cropping out in Apulia (adapted from Lepore et al. 2014)

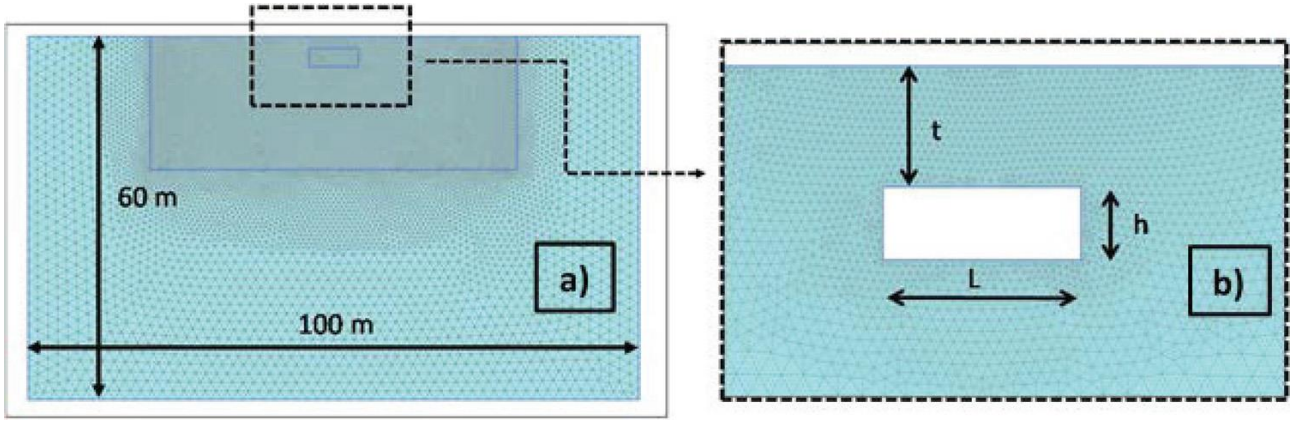

Fig. 2. (a) Geometry and discretization mesh adopted for the calculation domain; (b) geometrical parameters of the cavity (Note: h = cavity height; L = cavity width; t = overburden thickness)

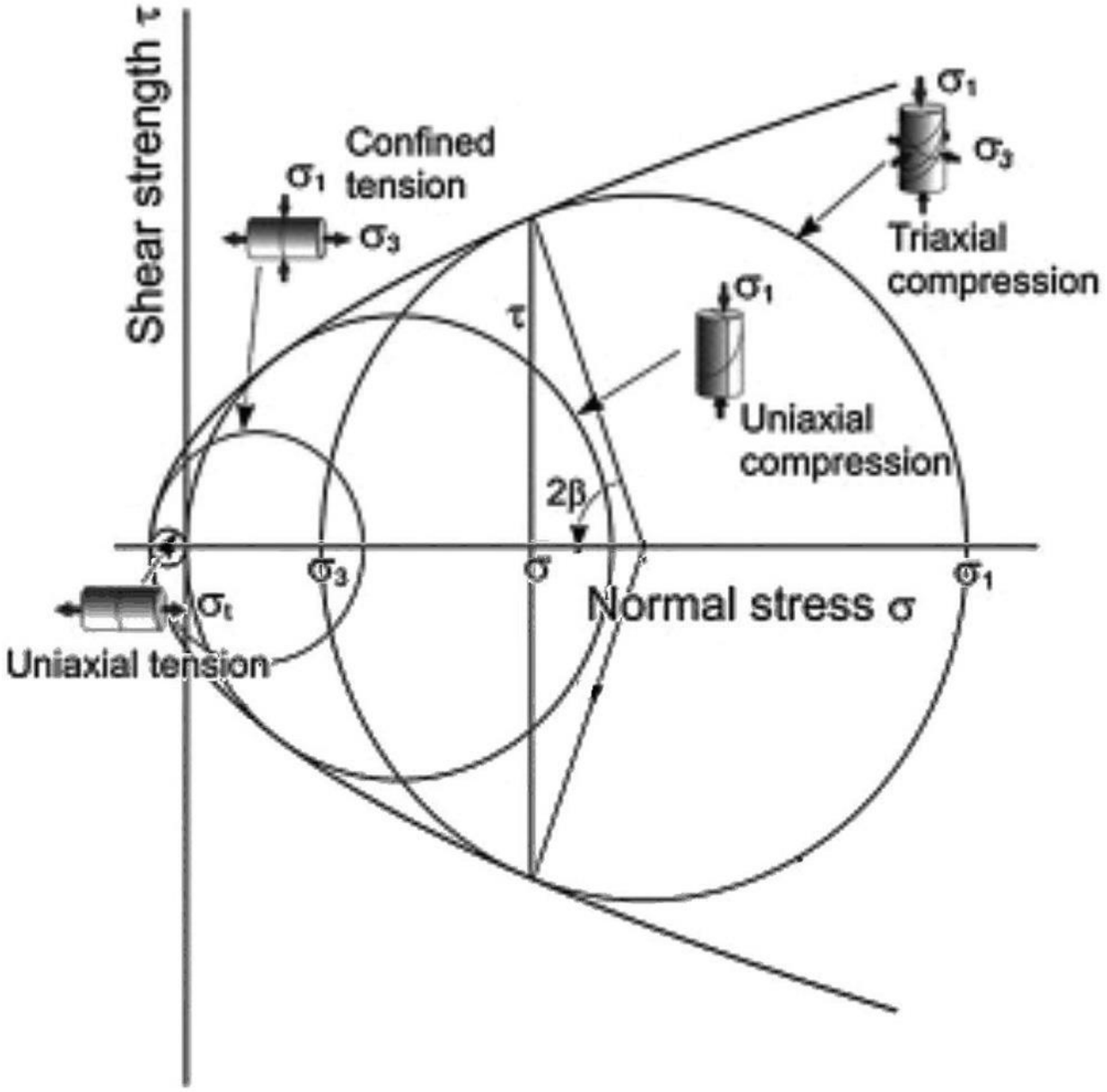

Fig. 3. Hoek-Brown strength envelope in Mohr's plane (adapted from Hoek and Martin 2014)

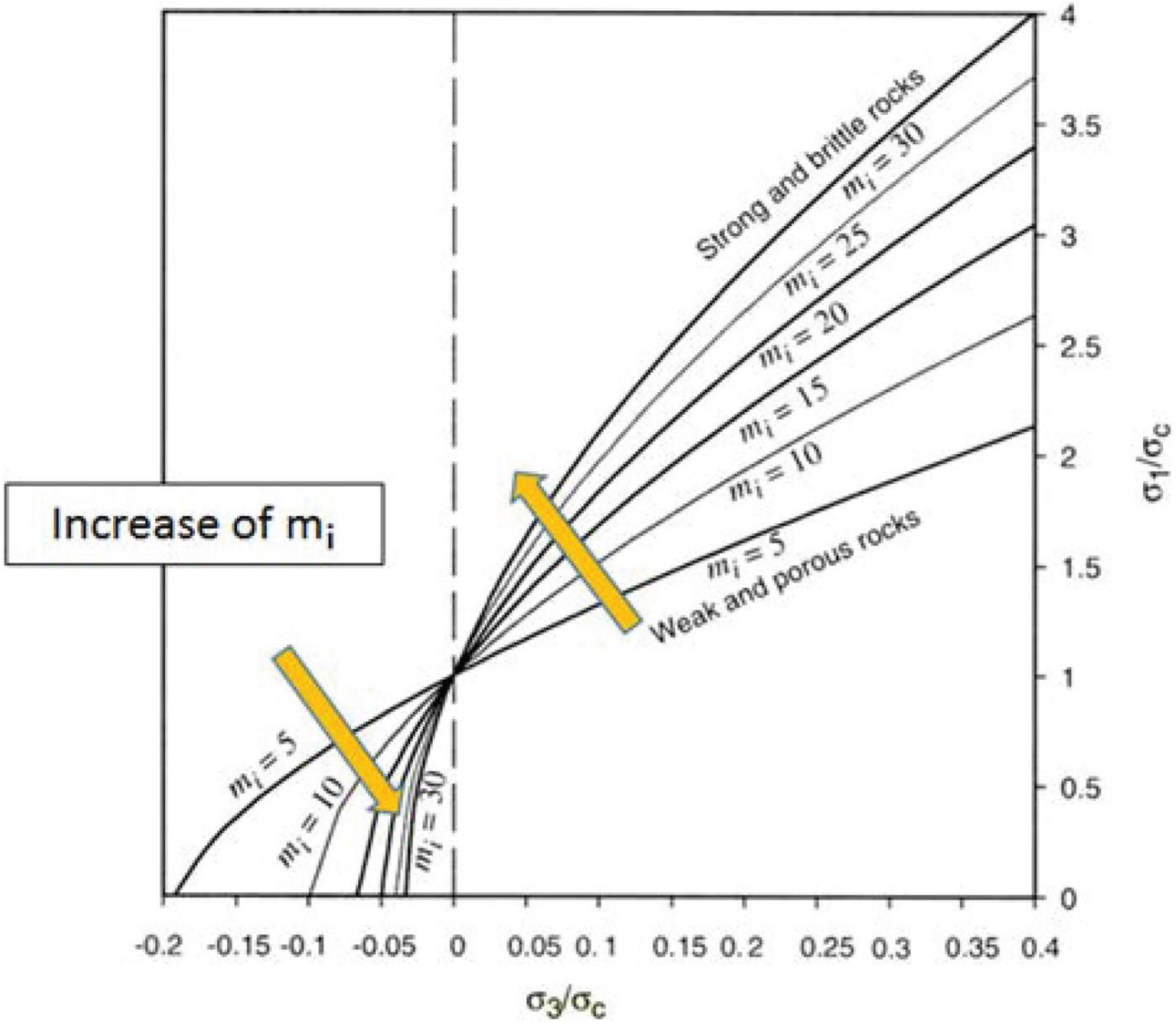

Fig. 4. Influence of the mi parameter on Hoek-Brown strength envelope (adapted from Cai 2010)

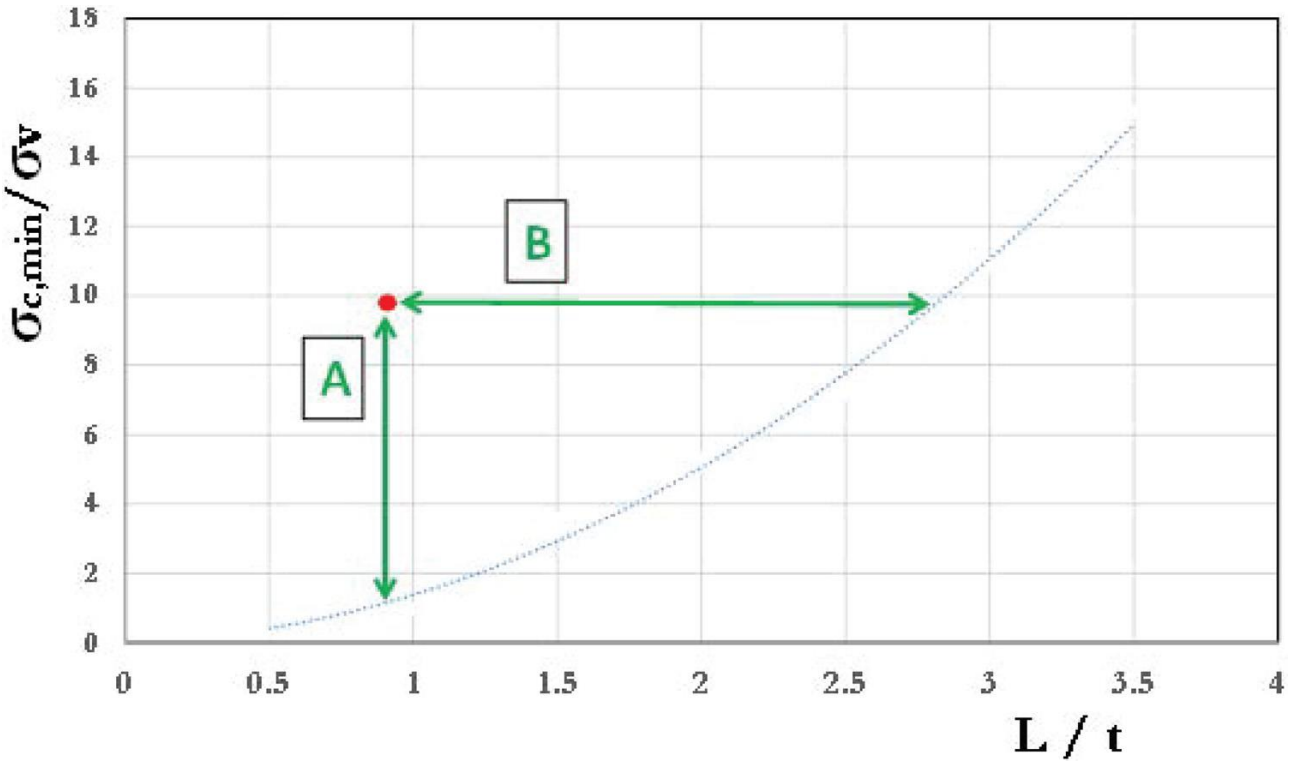

Fig. 5. Potential use of the chart for the assessment of cavity stability

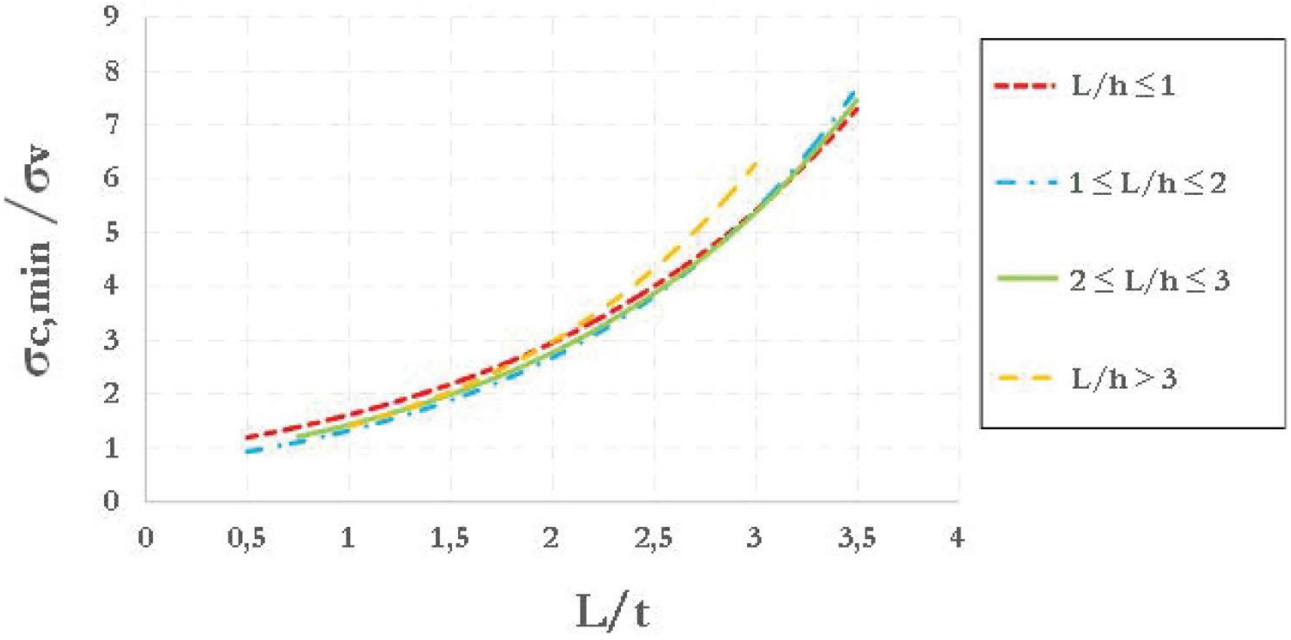

Fig. 6. Curves $\sigma_{c,min}/\sigma_v$ against L/t for different values of the ratio L/h ($m_i = 3$)

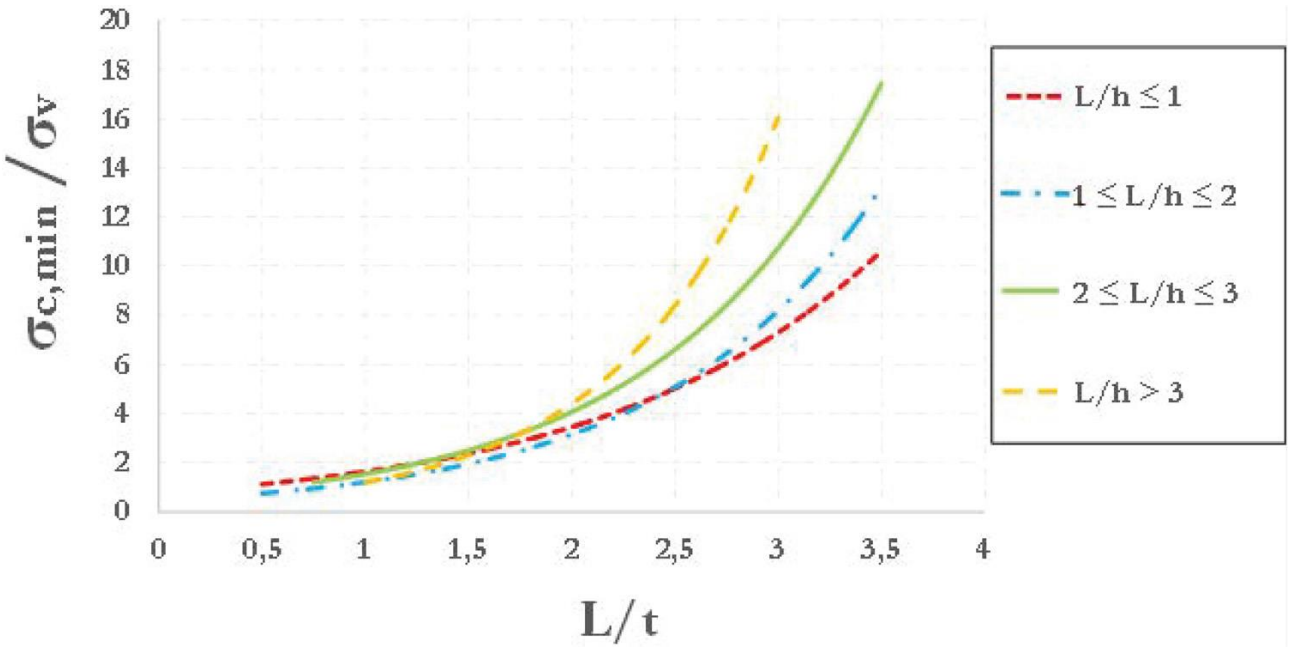

Fig. 7. Curves $\sigma_{c,min}/\sigma_v$ against L/t for different values of the ratio L/h (m_i = 8)

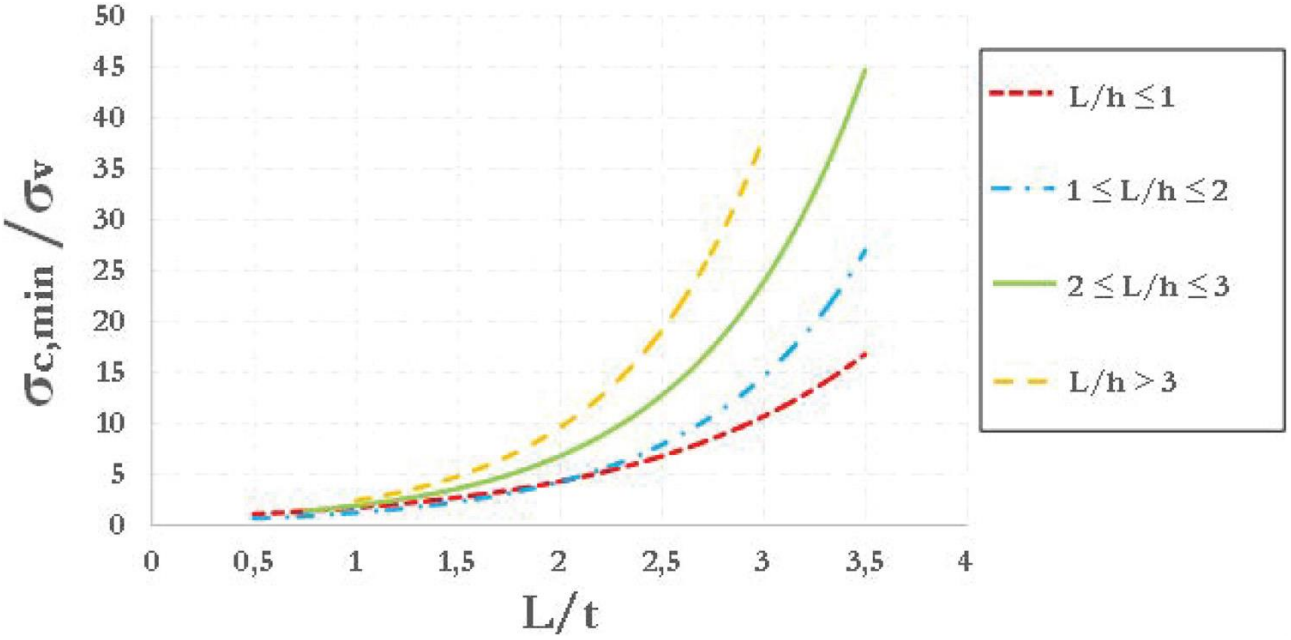

Fig. 8. Curves $\sigma_{c,min}/\sigma_v$ against L/t for different values of the ratio L/h (m_i =16)

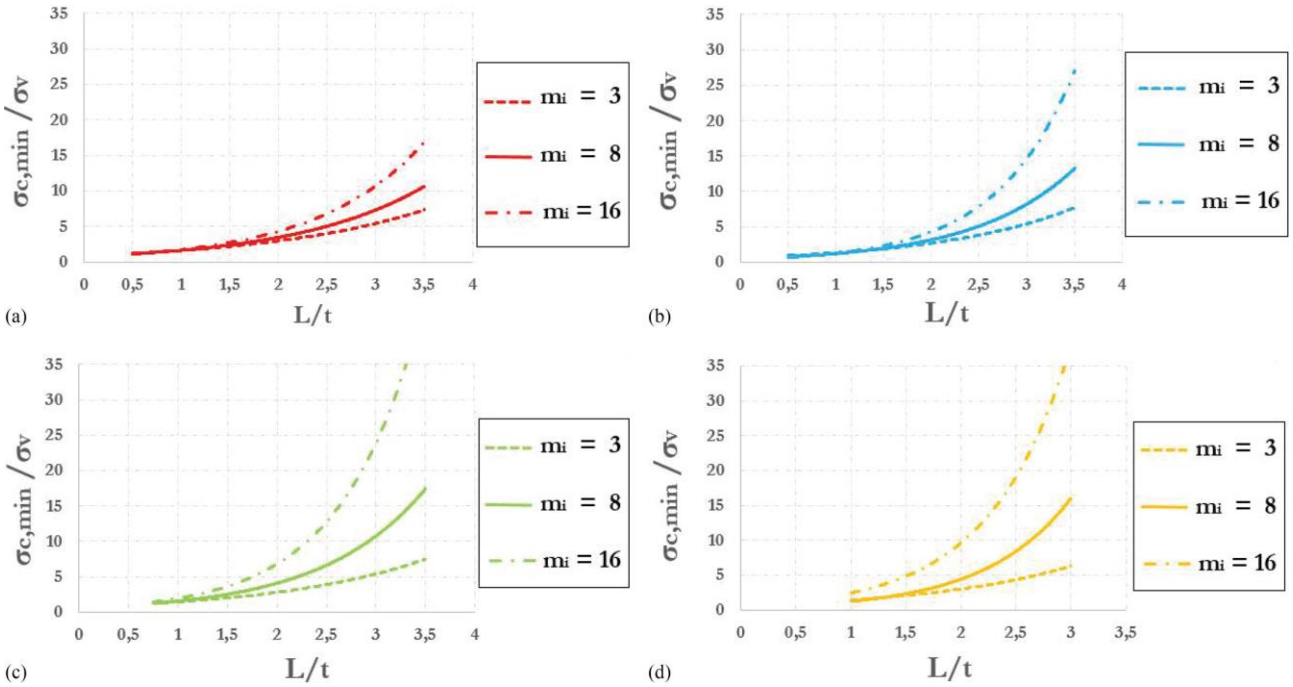

Fig. 9. Curves of $\sigma_{c,min}/\sigma_v$ against L/t for different values of mi: (a) $L/h \leq 1$; (b) $1 \leq L/h \leq 2$; (c) $2 \leq L/h \leq 3$; (d) $L/h \geq 3$

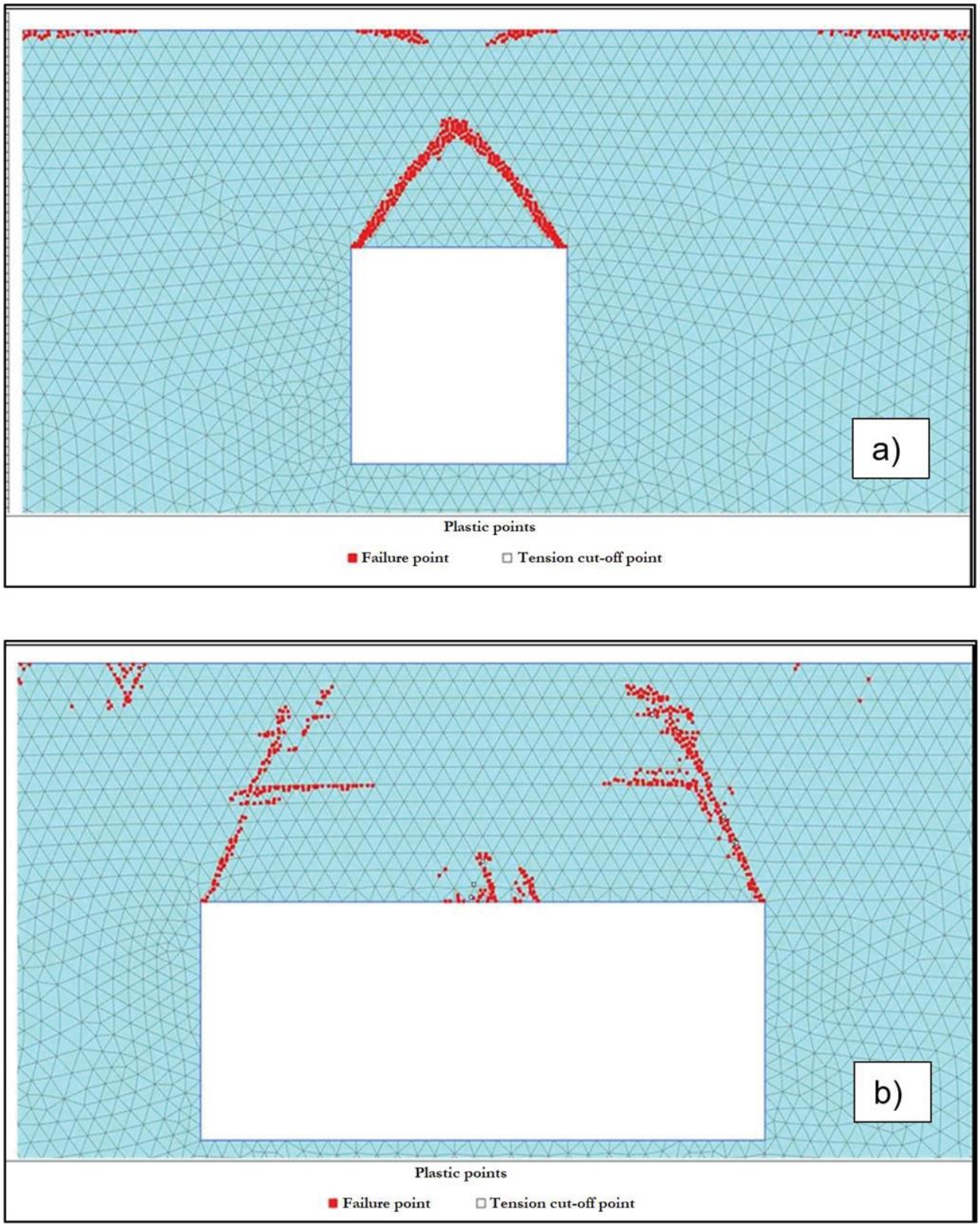

Fig. 10. (a) Arch-shaped general failure; (b) beam-shaped general failure

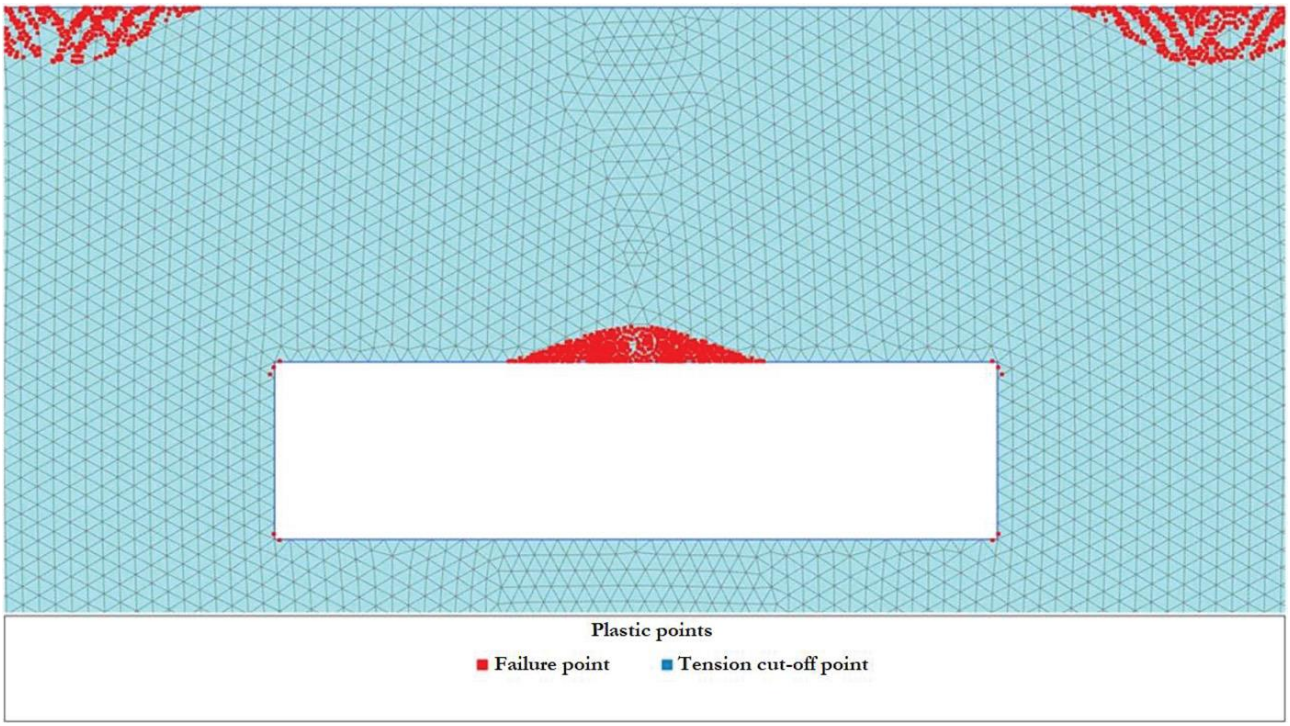

Fig. 11. Arch-shaped local failure

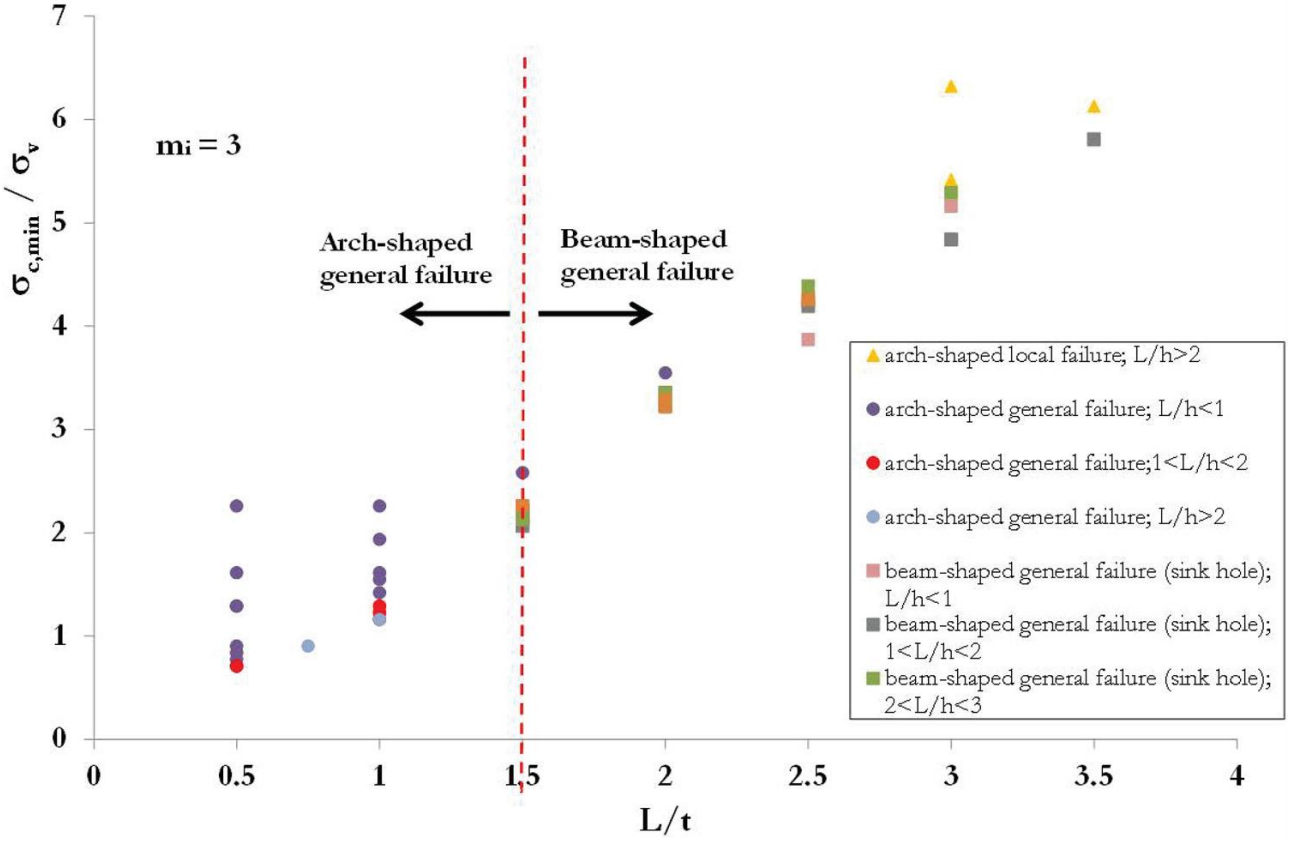

Fig. 12. Potential failure mechanism for a rectangular cavity as a function of the shape factor (L/h) and width-to-depth ratio (L/t) (mi = 3).

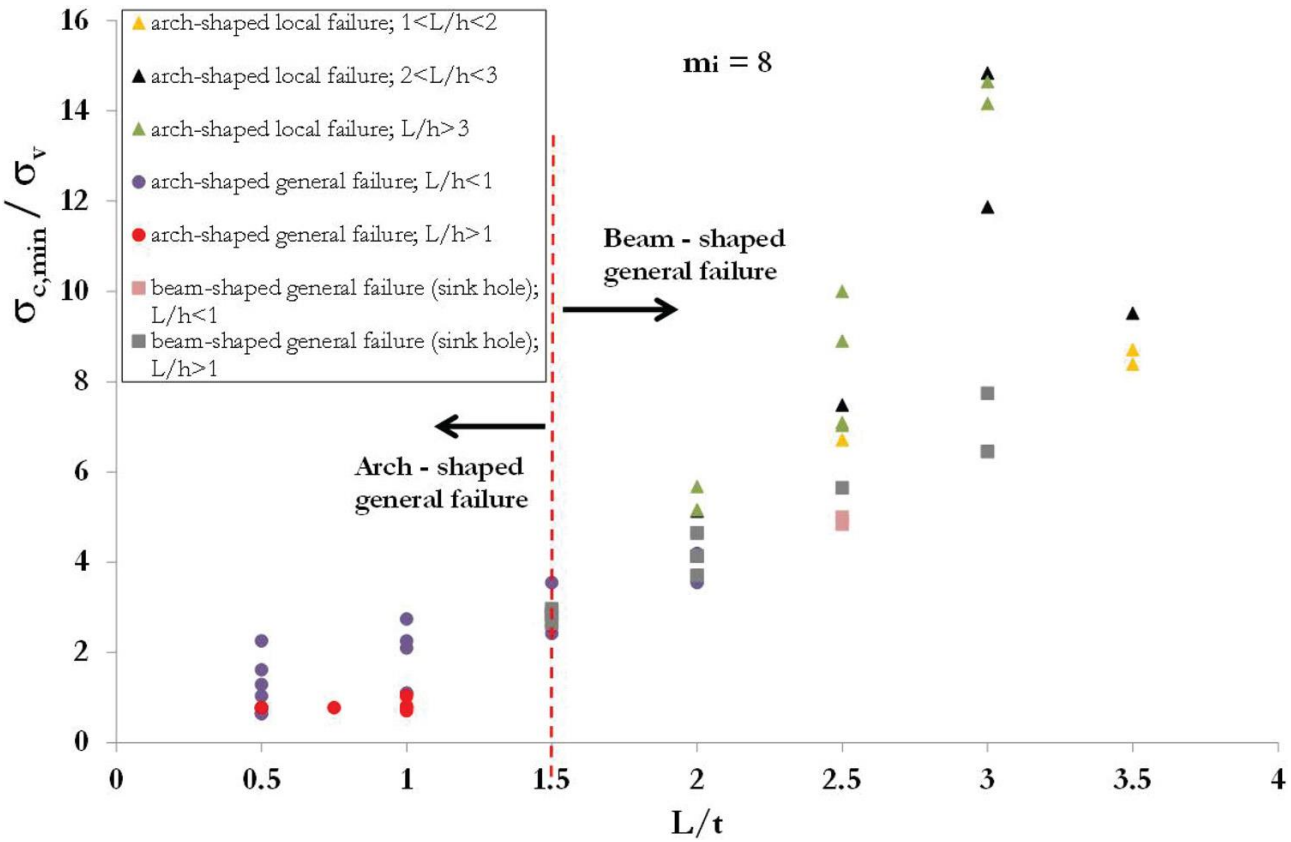

Fig. 13. Potential failure mechanism for a rectangular cavity as a function of the shape factor (L/h) and width-to-depth ratio (L/t) (mi = 8).

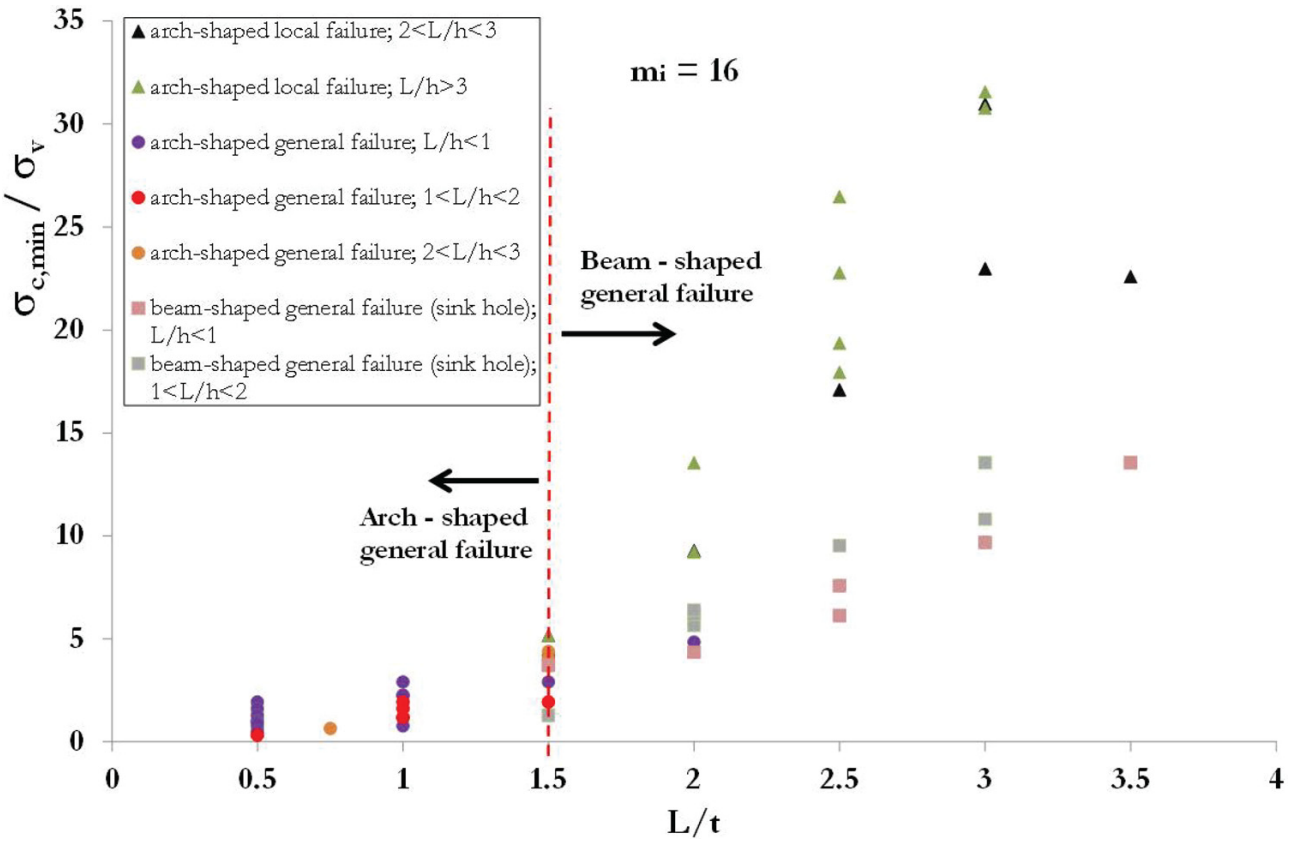

Fig. 14. Potential failure mechanism for a rectangular cavity as a function of the shape factor (L/h) and width-to-depth ratio (L/t) (mi = 16).

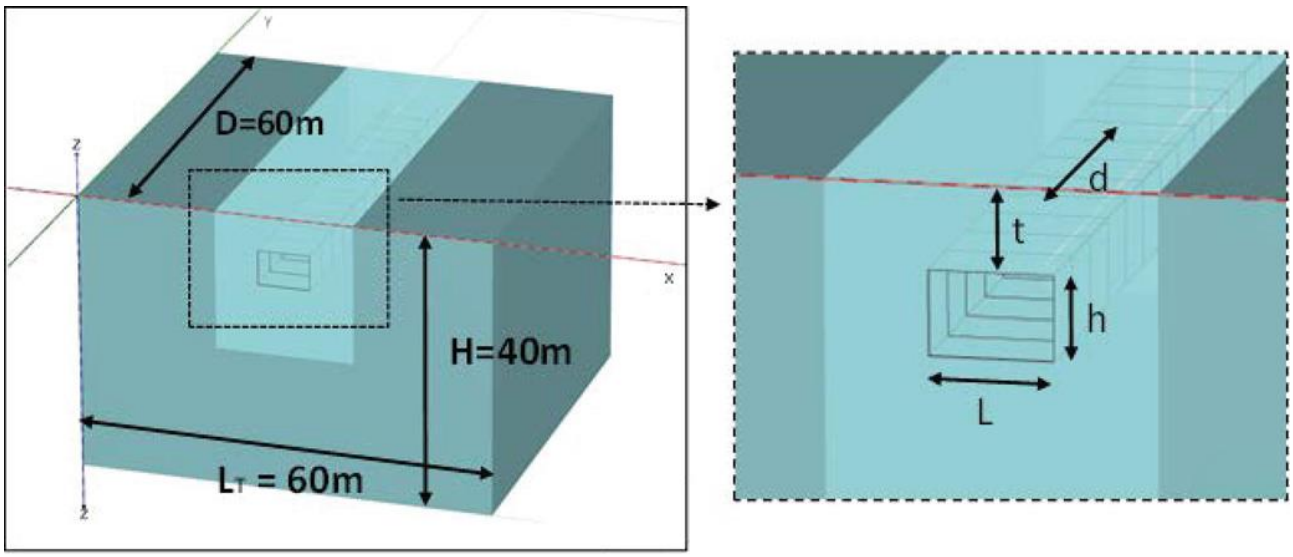

Fig. 15. (a) Calculation domain adopted for the 3D analyses; (b) details of the geometrical features of the cavity.

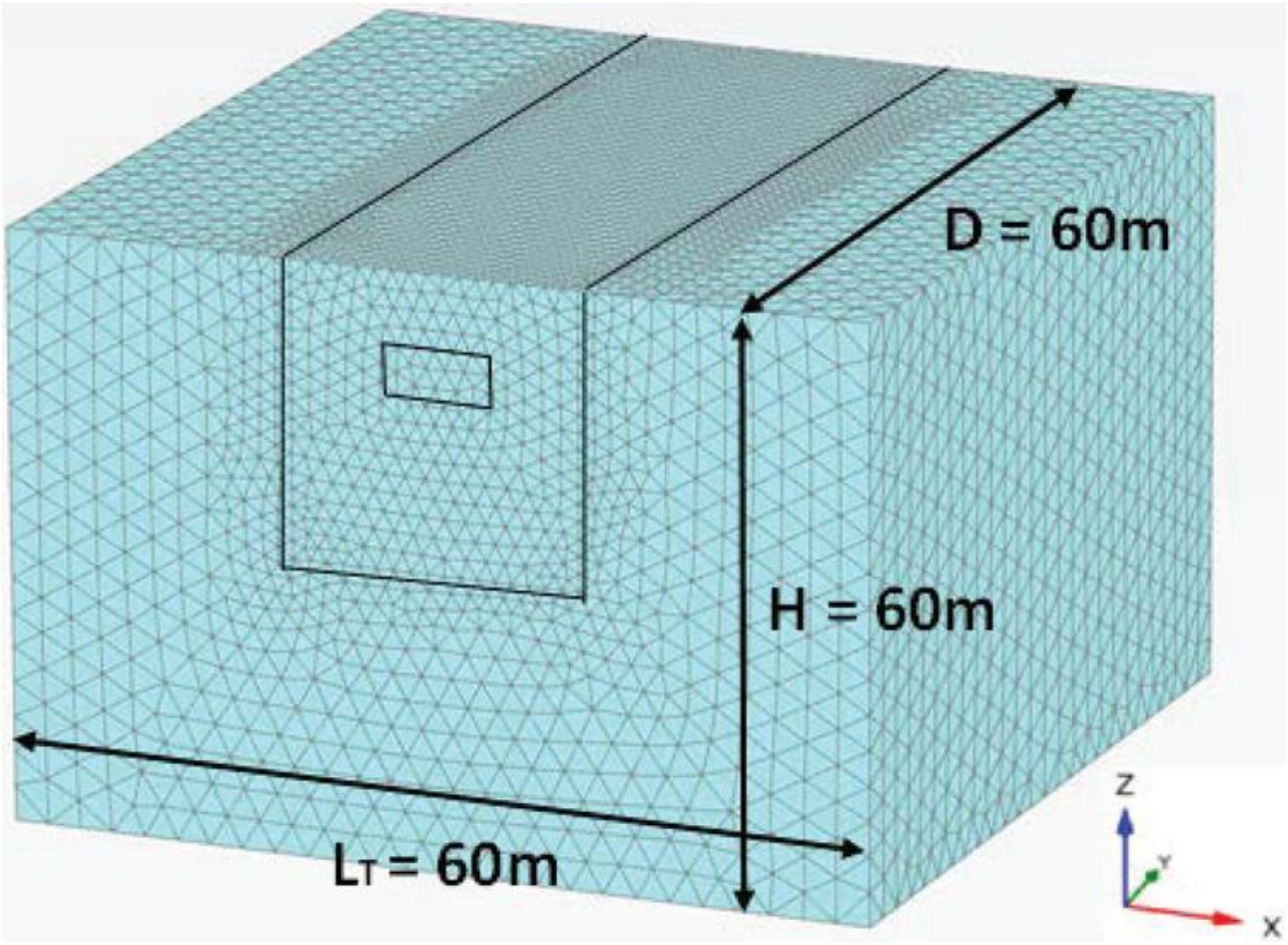

Fig. 16. Discretization mesh used for the 3D FEM analyses

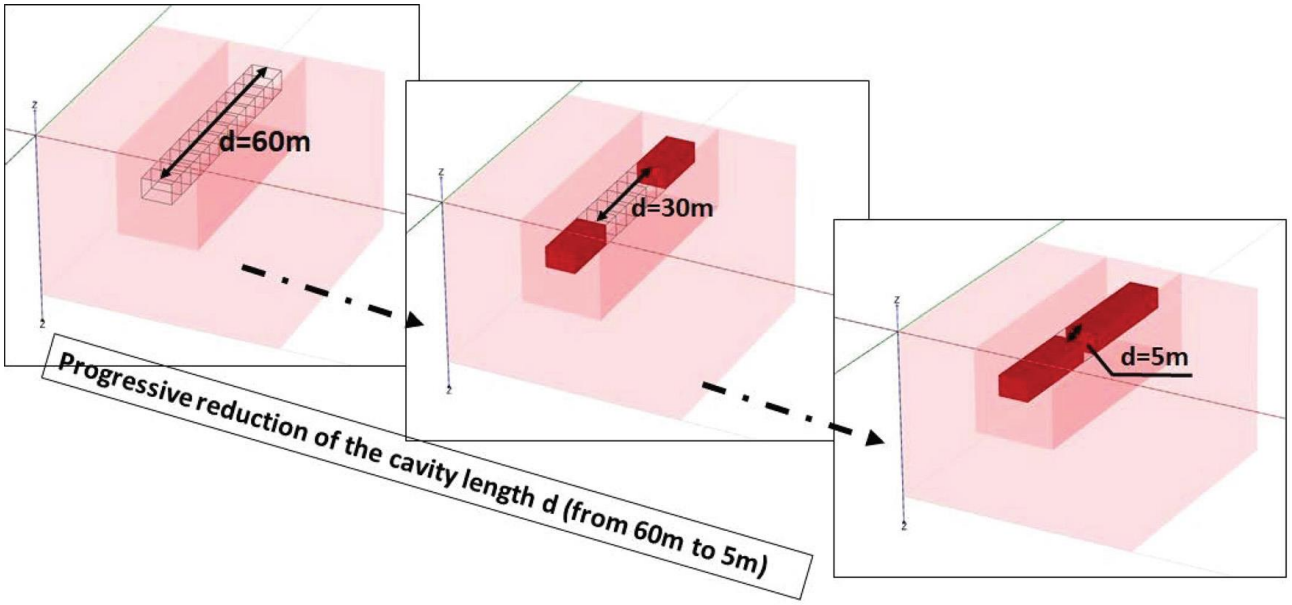

Fig. 17. Excavation simulation with progressive reduction of the cavity length (d) in the 3D FEM analyses.

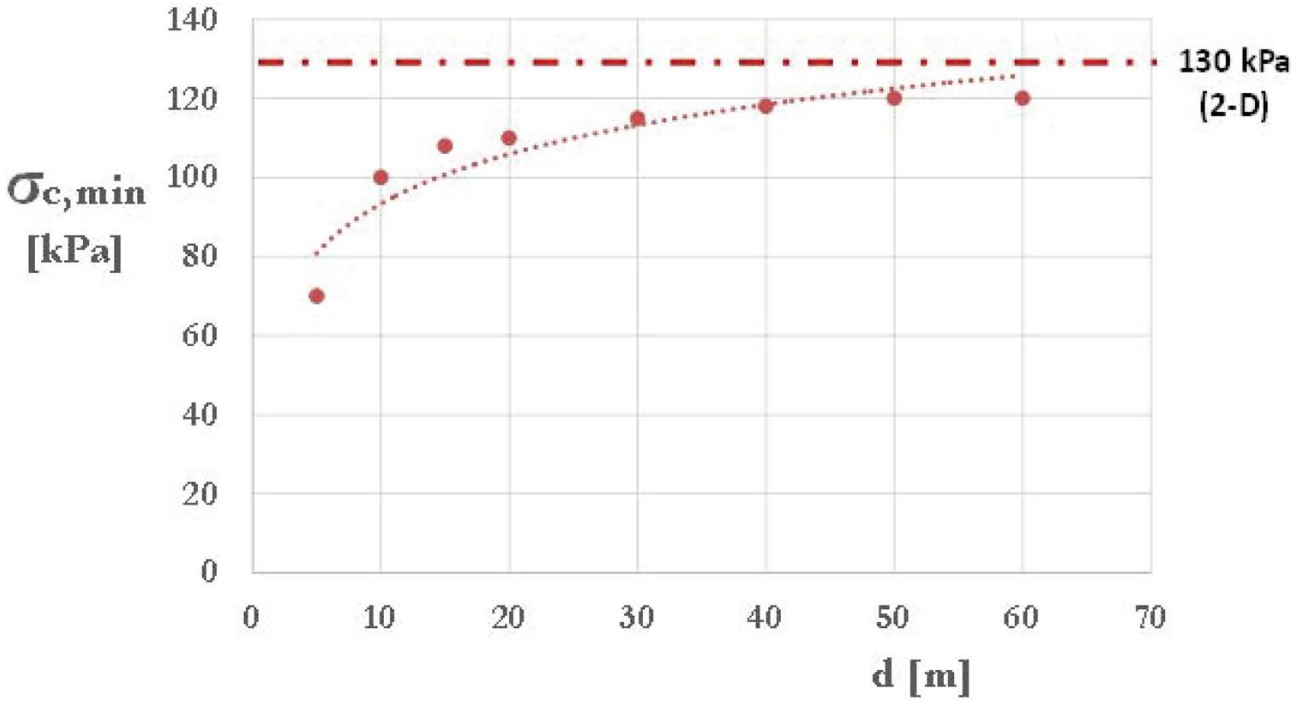

Fig. 18. 3D FEM analyses for squared-section cavity (L = h = 5 m): threshold uniaxial compressive strength ($\sigma_{c,min}$) against cavity length.

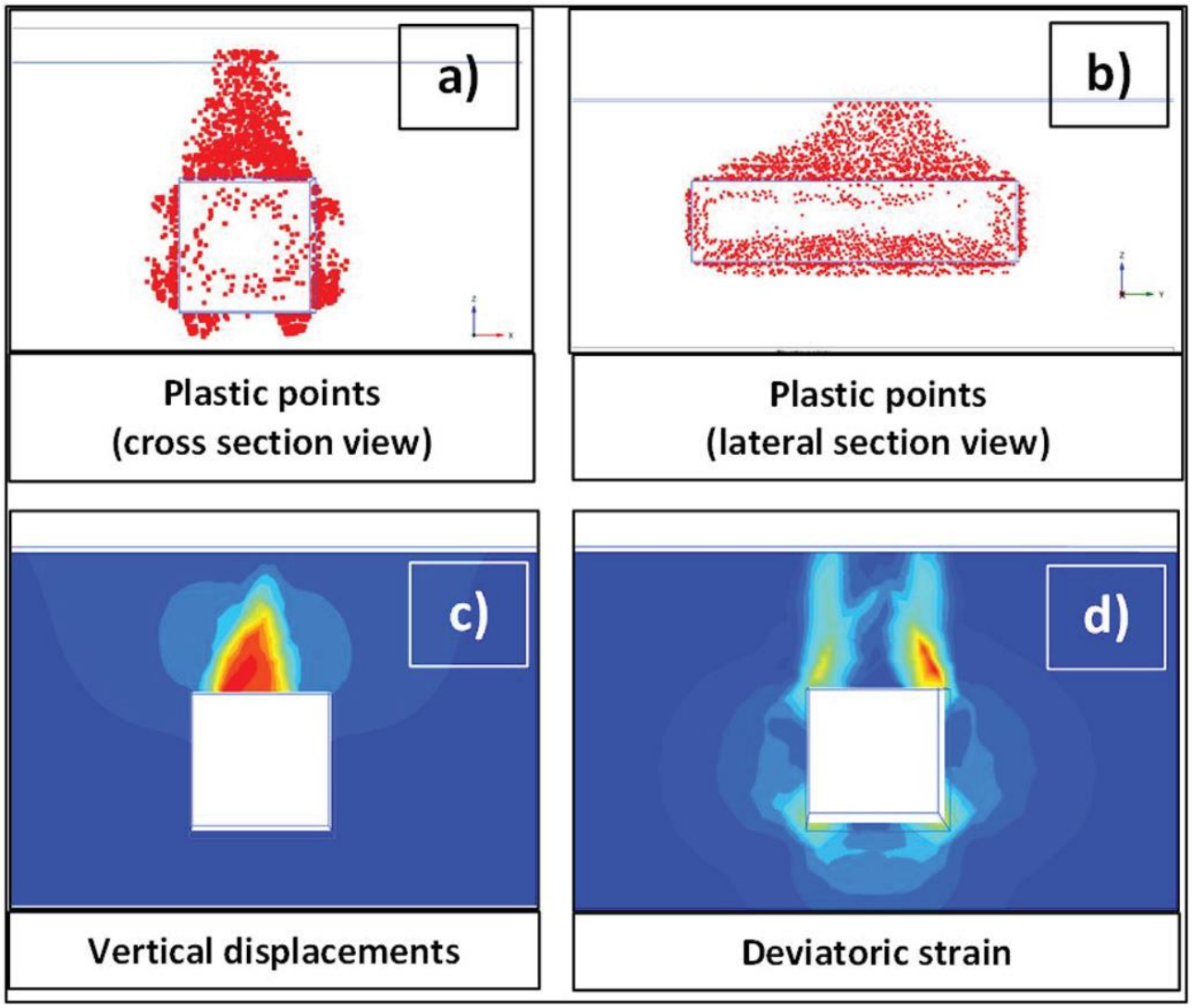

Fig. 19. Failure mechanism for a cavity with squared cross section (L = h = t = m): plastic points in (a) cross section and (b) lateral view; (c) vertical displacements and (d) deviatoric strain contours in cross section view.

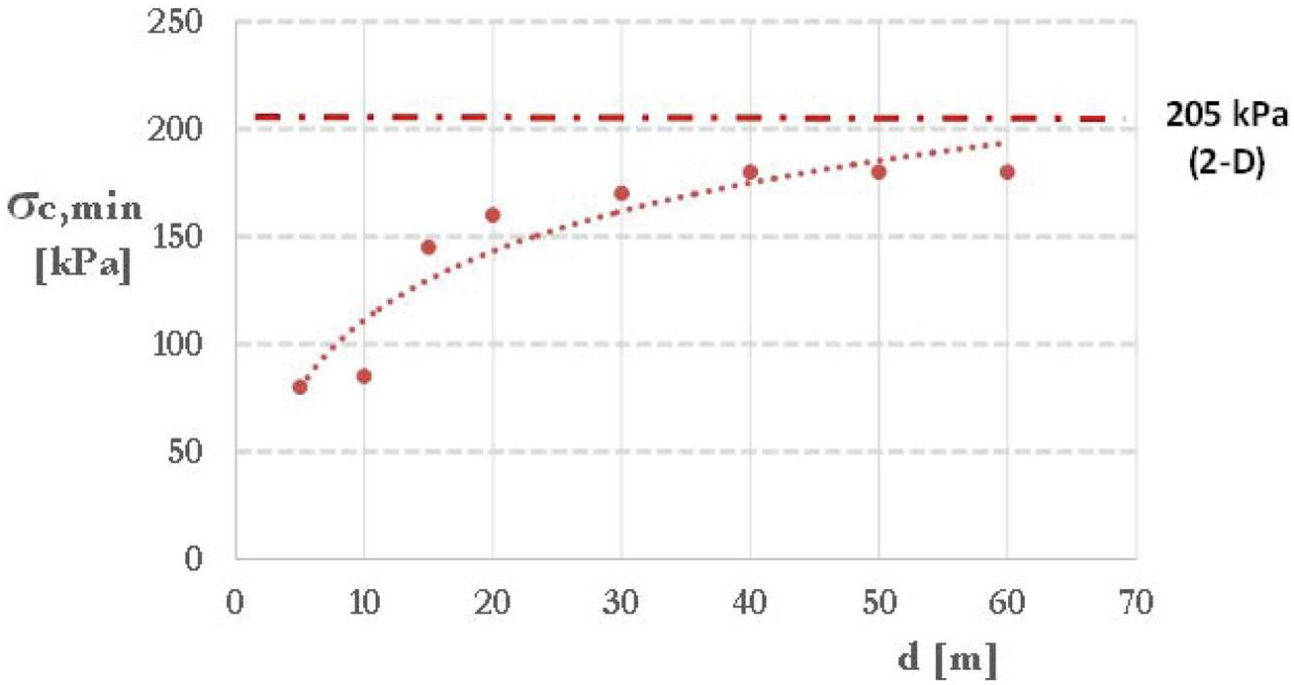

Fig. 20. 3D FEM analyses for a cavity with rectangular cross section (L = 7.5 m, h = 5 m): threshold uniaxial compressive strength ($\sigma_{c,min}$) against cavity length.

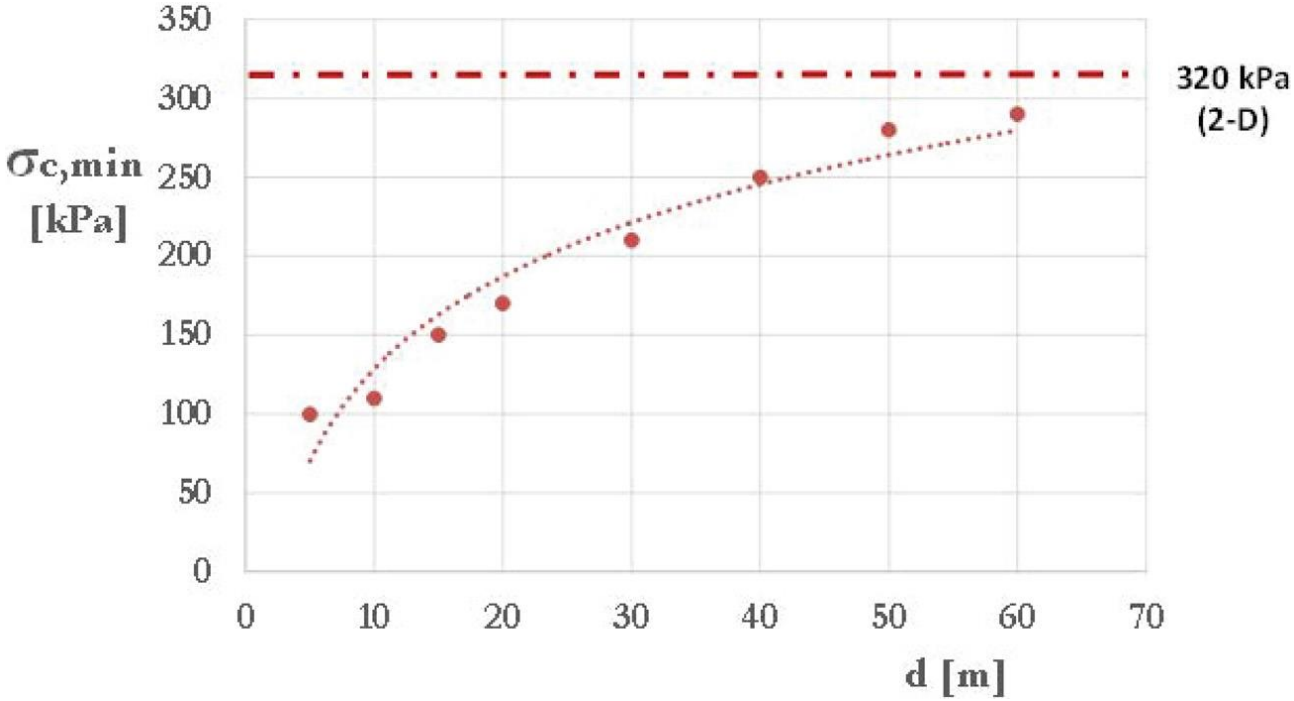

Fig. 21. 3D FEM analyses for a cavity with rectangular cross section (L = 10m, h = 5 m): threshold uniaxial compressive strength ($\sigma_{c,min}$) against cavity length.

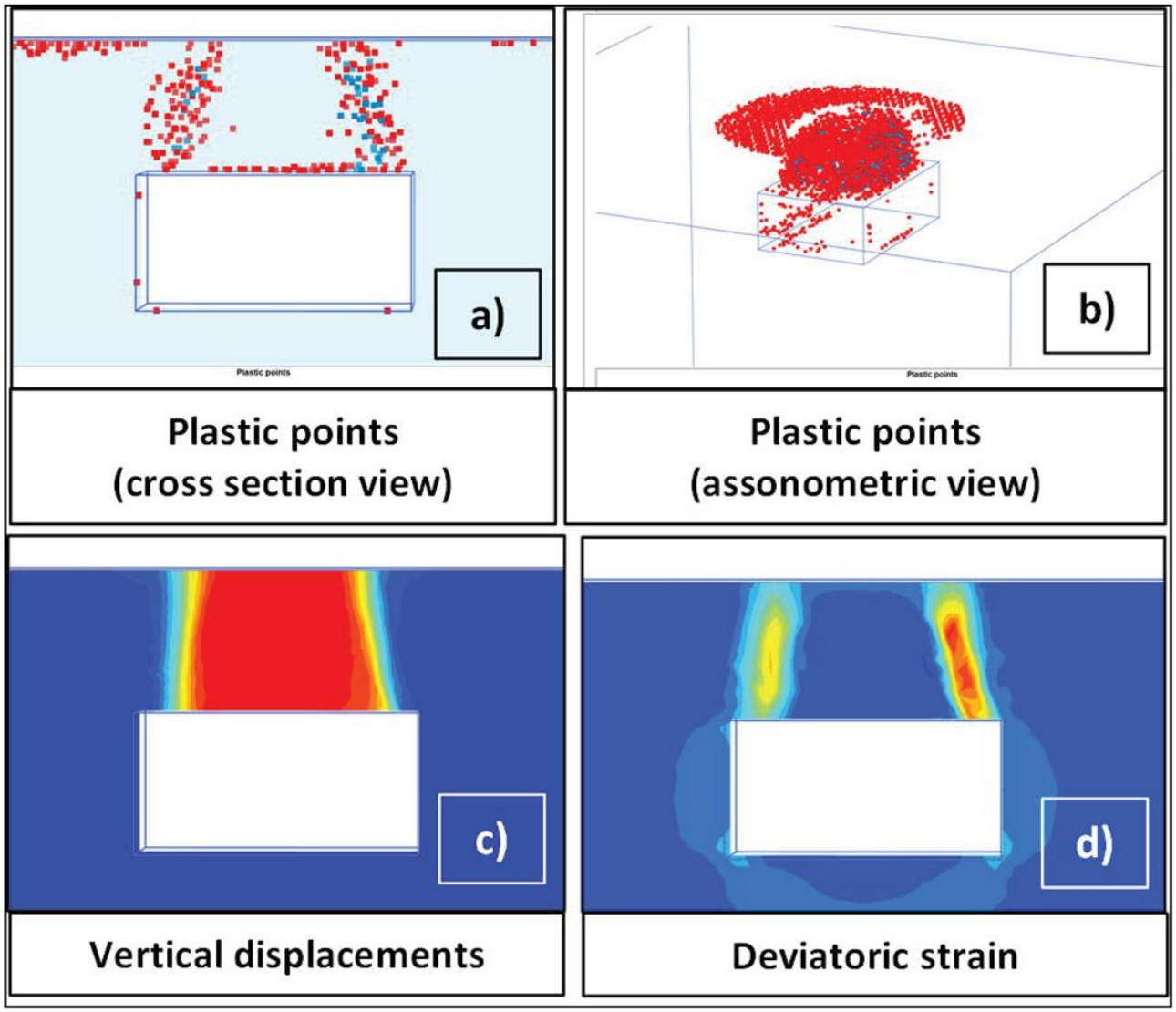

Fig. 22. Failure mechanism for a cavity with rectangular cross section (L = 10 m, h = 5 m, t = 5 m): plastic points in (a) cross section view and (b) assonometric view; (c) vertical displacements and (d) deviatoric strain contours in cross-section view